Variations in Tropical Sea Surface Temperature and Surface Wind Fields Associated with the Southern Oscillation/El Niño

EUGENE M. RASMUSSON AND THOMAS H. CARPENTER

Climate Analysis Center, NMC, NWS, NOAA, Washington, DC 20233

(Manuscript received 28 August 1981, in final form 21 December 1981)

ABSTRACT

Surface marine observations, satellite data, and station observations of surface pressure and precipitation are used to describe the evolution of sea surface temperature (SST) anomalies, surface wind fields, and precipitation anomaly patterns during major warm episodes in the eastern and central tropical Pacific. The sequence of events is described in terms of composite SST and wind fields (30°N–30°S) for six warm episodes since 1949, and time series and cross-spectral analyses of mean monthly data along six shipping lanes which cross the equator between the South American coast and 170°W.

During the months preceding a warm episode, the equatorial easterlies are stronger than normal west of the dateline. This and other coherent and strongly developed anomaly patterns over the western equatorial Pacific and South Pacific are associated with a South Pacific Convergence Zone (SPCZ) located southwest of its normal position. During October–November prior to El Niño, the equatorial easterly anomalies in the western Pacific are replaced by westerly anomalies. This change coincides with the appearance of positive SST anomalies in the vicinity of the equator near the dateline. East of the dateline (140–170°W), the wind anomalies along the equator follow a different pattern, with the diminution of the easterlies lagging rather than leading the development of positive SST anomalies near the Ecuador–Peru coast. Further south, SST's increase and the easterlies show a general decrease over most of the latitude band 10–30°S prior to the coastal warming.

Composites and cross-spectral analysis clearly show a westward migration of the eastern equatorial Pacific SST anomaly pattern from the South American coast into the central equatorial Pacific. Maximum SST anomalies typically occur around April–June along the South American coast, and near the end of the year around 170°W. This westward spread of positive SST anomalies coincides with the intensification of westerly wind anomalies along the equator and the development of anomalous northerly flow across the mean position of the Intertropical Convergence Zone (ITCZ). The southward shift of this convergence belt is accompanied by a northeastward shift of the SPCZ, resulting in a smaller wedge-shaped dry zone and enhanced precipitation in the eastern and central tropical Pacific. The surface wind anomaly field in the central equatorial Pacific is most strongly developed during August–December following the maximum SST anomalies along the Ecuador–Peru coast. During the northern winter following El Niño, the positive SST anomalies, as well as the low-level convergence and positive precipitation anomalies, are concentrated in the central equatorial Pacific. A simple calculation based on the surface divergence composite indicates that at this time enhanced large-scale vapor flux convergence in this area is comparable in magnitude to the enhanced precipitation.

The western end of a precipitation anomaly seesaw also appears in the data. Below normal precipitation is observed over Indonesia during the year of El Niño. Negative precipitation anomalies in the subtropics are associated with enhanced divergence and a weakened east Asian northeast winter monsoon in the Northern Hemisphere, and a weakened summer convergence zone east of Australia in the Southern Hemisphere.

1. Introduction

The interannual variability of sea surface temperature (SST) along the Peru–Ecuador coast is dominated by the El Niño phenomenon. The name El Niño was originally applied to a weak warm coastal current which annually runs southward along the coast of Ecuador around the Christmas season (Wyrtki, 1975). In scientific usage, the term has now become more narrowly associated with the more extreme warmings which occur every few years (Wyrtki, 1979a), and which result in catastrophic effects on the ecological system of the region. In more recent years, Ramage (1975), Weare *et al.* (1976), and others have used the term to encompass the larger-scale features of the warming event, i.e., the upwelling area along both the equator and the South American coast.

These warm episodes exhibit a wide spectrum of amplitudes, as well as variations in character and timing. Thus, Wyrtki (1975) and Ramage (1975) list three "major" El Niño events (1957, 1965, 1972) during the period 1950–73. During the same period, Wooster and Guillen (1974) identify three additional minor El Niño's (1951, 1953, 1969). Quinn *et al.* (1978) classified El Niño's as strong, moderate,

weak, and very weak. Their expanded list includes the 1963 event and the 1975 "aborted" event in the very weak category.

The relationship between warm SST episodes in the eastern equatorial Pacific and global-scale climate variations is best viewed within the framework of the Southern Oscillation (SO). Nearly a century ago, Hildebrandsson (1897) uncovered the first hint of the SO in the form of an out-of-phase relationship between surface pressure anomalies at Sydney and Buenos Aires. Five years later Lockyer and Lockyer (1902a) confirmed the existence of the Sydney–Buenos Aires pressure seesaw, and estimated its period to be ~3.8 years. More extensive analyses (Lockyer and Lockyer, 1902b, 1904) revealed the oscillation to be almost global in extent.[1]

It remained, however, for Sir Gilbert Walker, in a classical series of papers (Walker, 1923, 1924, 1928; Walker and Bliss, 1930, 1932, 1937) to name the SO and describe the salient features of the surface pressure, temperature and precipitation fluctuations. Quoting Walker and Bliss (1932): "When pressure is high in the Pacific Ocean it tends to be low in the Indian Ocean from Africa to Australia; these conditions are associated with low temperatures in both these areas, and rainfall varies in the opposite direction to pressure. Conditions are related differently in winter and summer, and it is therefore necessary to examine separately the seasons December to February and June to August."

Except for the work of Berlage (1957, 1966) and Troup (1965), only limited attention was given the SO from the time of Walker to the mid-1960's. A renewed surge of interest developed in the late 1960's when it became apparent that the interannual SST variations in the eastern tropical Pacific were closely linked with the SO, thus introducing the ocean as the possible memory mechanism for the oscillation.

Early evidence of a link between the SO and El Niño was provided by Berlage (1966), who noted a strong relationship between interannual surface pressure variations at Djakarta and SST at Puerto Chicama on the Peru coast. About the same time, Doberitz (1968) documented the positive correlation between SST and rainfall in the equatorial Pacific dry zone. However, it was the remarkable synthesis by Bjerknes (1966, 1969, 1972) which clearly linked the interannual fluctuations in SST over the broad expanse of the eastern equatorial Pacific, with SO-related changes in the zonal wind component near the equator (the Walker Circulation) and the large-scale equatorial Pacific precipitation regime. Bjerknes' work also provided strong evidence of links (teleconnections) between the equatorial Pacific and the Northern Hemisphere westerlies. His studies marked a shift in emphasis from statistical analysis of the SO to more physically-oriented diagnostic studies, e.g. Krueger and Gray (1969), Krueger and Winston (1974, 1975), in which satellite data provided an important new source of information.

Kidson (1975) identified the SO with the first eigenvector of the normalized non-seasonal fluctuations of temperature and precipitation in the tropics (30°N–30°S), and with the first eigenvector of the global surface pressure fluctuations. Trenberth (1976) pointed out the important role of the South Pacific Convergence Zone (SPCZ) in the SO. Namias (1976) provided further observational evidence of atmospheric teleconnections between the equatorial and North Pacific regions. A significant new dimension of the SO/El Niño was uncovered by Wyrtki (1975), when he showed that El Niño events are associated with changes in the east–west slope of sea-level in the tropical Pacific.

In a logical extension of the empirical studies, Rowntree (1972), Julian and Chervin (1978), and more recently, Keshavamurty (1982) used general circulation models to study the response of the atmosphere to a fixed SST anomaly in the tropical Pacific. The problem of ocean–atmosphere interactive coupling involving SST and Walker Circulations has been studied theoretically by McWilliams and Gent (1978) and Lau (1981) using simple idealized models. Recent experiments by Opsteegh and van den Dool (1980), Hoskins and Karoly (1981) and Webster (1981), using relatively simple linear, steady-state models designed to study the response of the atmosphere to thermal and orographic forcing, have provided insight into some of the basic processes of local and remote forcing, and qualitatively reproduced some of the features of the observed teleconnection patterns.

Horel and Wallace (1981) recently examined the vertical structure of atmospheric SO fluctuations and extratropical teleconnections. They found the zonally-averaged 200 mb SO height fluctuations to be considerably larger than those at the 1000 mb level. Corresponding fluctuations in the mean temperature of the tropical troposphere are on the order of 1°C.

[1] In the 1904 paper is a map of the pressure oscillation which is quite similar in its gross aspects to the map of worldwide annual average surface pressure correlations with Djakarta, prepared a half century later by Berlage (1957).

In a later paper, Lockyer (1906) succinctly summed up the results of the earlier work in the following words: "In a paper communicated to the society in the year 1902, Sir Norman Lockyer and I pointed out the existence of a barometric see-saw of short duration (about 3.8 years) occurring between two large regions, nearly antipodal to each other, the centers of which were approximately India and Cordoba (South America). A continuation of the research indicated that this barometric see-saw was of greater extent than was at first supposed, and in a further communication in the same year observations extending over new regions were discussed and the results published. Still further inquiry indicated that this see-saw was almost world-wide in its extent, and the result of a later investigation, which included the examination of pressure observations at 95 stations scattered over the earth's surface, was communicated to the society in the year 1904."

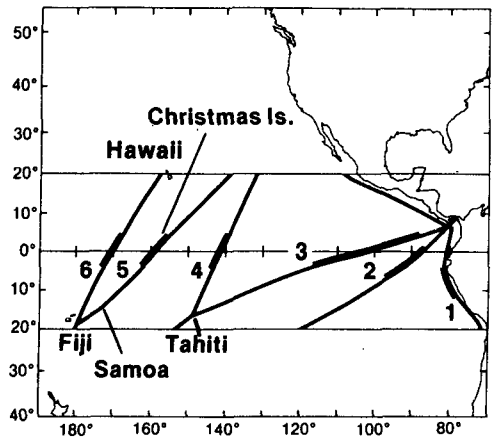

FIG. 1. Ship tracks used in the analyses. The heavy portion of each track is the 8° latitude section of maximum interannual SST variability. The time series of monthly average anomalies were computed for this section of each track.

Well-defined teleconnection patterns were found in the Northern Hemisphere height fields, and a theoretical explanation for these patterns based on Rossby wave propagation on a sphere (Hoskins and Karoly, 1981; Webster, 1981), was proposed. Van Loon and Madden (1981) have also found evidence of a well defined pattern of SO teleconnections in the Southern Hemisphere extratropics.

Additional studies during the past decade will be cited in their appropriate context. Although these efforts have provided significant new information and insight into the behavior of the SO, this fascinating system of ocean–atmosphere climate variations is still inadequately described, and even more poorly understood.

The results of a study of SO-related variations in SST and surface wind fields over the tropical Pacific are described in this paper, which represents one part of a more comprehensive descriptive study of SO fluctuations conducted by ourselves and our colleagues. Other aspects of the study include upper-air teleconnections (Arkin *et al.*, 1980), and large-scale variations in precipitation (Heddinghaus and Krueger, 1981).

The data sets used in this study are described in Section 2. The conventional Southern Oscillation Index (SOI) is usually computed as the difference between station pressures representing the opposite centers of the Indonesian–South Pacific pressure seesaw. The relationship between this index and SST variations along the Ecuador–Peru Coast is documented in Section 3.

Section 4a contains a brief description of some aspects of the seasonal cycle of SST and surface wind in the tropical Pacific. Warm episodes along the South American Coast are described in Section 4b. SST lag relationships in the eastern tropical Pacific, as well as local relationships between SST and wind variations, are examined in Section 4c, using data along six ship tracks which cross the equator between the South American coast and 170°W.

A composite description of the morphology of a warm episode, as manifested in the SST and surface wind fields of the tropical Pacific (30°N–30°S), is presented in Section 5. The major findings and conclusions are discussed and summarized in Section 6.

2. Data and computations

A new data set of surface marine wind and SST observations for the Pacific Ocean, spanning the period 1854–1976, was assembled by the National Climatic Center (NCC) specifically for this project. The individual sources from which data were obtained are listed in the Appendix.

Duplicate observations were identified and eliminated. Preliminary quality assurance was handled through programs that checked for internal consistency and climatic limits. The data were then arranged into frequency and cumulative relative frequency class intervals and manually reviewed.

The post-World War II data used in this study are almost entirely intake observations. For earlier periods, we chose to use only the bucket observations. Analyses by Saur (1963) and Tabata (1978) show that mean differences between bucket and intake temperatures vary from one cruise to another, and from one ship to another. Saur (1963) calculated a mean "bucket minus intake" difference of −0.7°C from 6800 pairs of observations. Collins *et al.* (1975) found a mean difference of −0.3°C between Canadian ship intake observations and Japanese merchant vessel bucket observations, which they attribute to intake heating. An analysis of differences between bucket and intake SST observations in our data indicated a probable positive bias of around 0.3 to 0.5°C in the intake data, but the bias did not appear to be constant in time and space, and is not large enough to significantly affect our main conclusions. Nevertheless, this bias should be kept in mind when comparing SST data from the post- and pre-World War II periods.

Two additional summary data sets were prepared: 1) Mean monthly values for each 2 × 2° latitude–longitude square of the Pacific between 30°N–30°S covering the period 1946–76, and 2) mean-monthly values for 1° latitude × 5° longitude strips between 20°N–20°S along six shipping lanes which cross the equator between the South American Coast and 170°W (Fig. 1), covering the periods 1921–38, and 1946–76. Further quality control was performed for each sub-area of these data sets. Initial long-term mean values and standard deviations (sigma) were computed for each calendar month for SST, and westerly (U) and southerly (V) wind components. A

four-pass editing procedure was then applied. On each pass, values of SST outside the ±3.56 sigma limits for all data from that particular calendar month were removed, and a new long-term mean and sigma computed. The level of discard is believed to be a conservative one, retaining almost all the good data at the expense of passing a few erroneous observations.

Wyrtki and Meyers (1976) have demonstrated that even with little editing, important information on interannual variability can be extracted from the surface wind data. We applied a quality control procedure in which the wind components were treated as components of a bivariate normal distribution, thus allowing consideration of the total wind vector in the editing sequence. A four-pass editing procedure was again adopted with observations outside a chi-square limit of 15.2 discarded after each pass.

One additional data set was derived from the ship track data. This consisted of monthly averaged values of SST, U, and V for the 8° latitude strip along each ship track which exhibited the greatest interannual variability of SST (Fig. 1). Prior to constructing the averages, the individual monthly values along the ship track were filtered first in latitude, then in time, using a nonlinear filter (Rabiner *et al.*, 1975). This filter involves a combination of median smoothing passes, and is extremely effective in removing isolated wild points without appreciably smoothing valleys, peaks, or sharp discontinuities. For those few months when data were missing from all eight 1° strips, the anomaly was estimated by linear interpolation between adjacent months. These data gaps never exceeded three months, and no interpolations were necessary for the track along the South American Coast (Ship Track 1).

For details of the Fast Fourier Transform techniques used to obtain the spectra and cross-spectra in Sections 3 and 4, see Rasmusson *et al.* (1981). All spectra and cross-spectra are derived from unsmoothed mean monthly values spanning the 256 month period September 1953–December 1974. Ten percent of the data on either end of the series were multiplied by a cosine taper to reduce leakage. The raw spectral estimates and the cross-spectral values were smoothed using three-point and seven-point running means, respectively. Thus, every third spectral estimate and every seventh coherence square value shown on the plots represents an independent estimate with 5.2 and 12.2 effective degrees of freedom, respectively (Julian, 1971, 1975).

It is pointed out in Section 3 that the SO is aperiodic. Spectra of its various components are often quite different from one period to another. Although the oscillation happens to be quite sharply peaked around periods of 36.6–42.7 months during the 22-year period being analyzed, this is not necessarily true for other periods, and we do not consider it profitable to dwell on the statistical significance of this SO peak. Rather, we are interested in the temporal and spatial relationships between various parts of the oscillation, i.e., the level of significance of the coherence square and phase spectra in the SO frequency range. The 95% (0.44), 99% (0.59) and 99.9% (0.74) levels of significance (Julian, 1975) are indicated on the coherence square plots. Confidence limits for phase differences are not indicated, but are discussed. These are obtained from Jenkins and Watts (1968).

3. The Southern Oscillation Index and SST variations along the South American coast

Until recently most investigators have examined the SO largely in the context of a standing oscillation. This assumption is implied in the use of unlagged data from widely separated stations to form an SOI. Trenberth (1976) however, called attention to phase differences of a few months in the pressure oscillations over the Australian–South Pacific region. Chen (1982) performed a cross-spectral analysis of the mean monthly surface pressure anomaly time series for Darwin (12.4°S, 130.9°E), Easter Island (27.2°S, 109.4°W), Rapa (27.6°S, 144.3°W) and Tahiti (17.5°S, 149.6°W), and confirmed the lags noted by Trenberth (1976). For the period analyzed, the lag in the out-of-phase variation between Darwin and Tahiti was about one month (Tahiti leading). The lag between Rapa and Easter Island was about one month (Rapa leading), and these two stations led Tahiti and opposite changes at Darwin by several months. Chen's results imply that surface pressure changes near the axis of the South Pacific High (Rapa, Easter Island) lead those at lower latitudes in the central Pacific (Tahiti), and lead changes of opposite sign in the vicinity of the Australian–Indonesian Low (Darwin). The conventional surface pressure index monitors only one aspect of the SO. One might also index other fluctuations such as the strength of the equatorial easterlies (Wyrtki, 1980), upper tropospheric flow over the equator (Arkin *et al.*, 1980), rainfall variations in the Central Pacific (Reiter, 1978) or SST. Since this paper is focused on large-scale SST variations in the eastern and central equatorial Pacific, we chose as the reference for much of our subsequent discussion the average SST anomalies near the upper Peru Coast (4–12°S) as reflected by the data from Ship Track 1 (Fig. 1). The spectrum for this index, which will be referred to as SST(1), is shown in Fig. 2, along with two of Chen's SO indices. All spectra exhibit major peaks at periods ~36.6–42.7 months, which define the dominant SO period during these years (1953–74). However, SST anomalies in this area exhibit far more month-to-month persistence than do the surface pressure anomalies; thus a higher percentage of

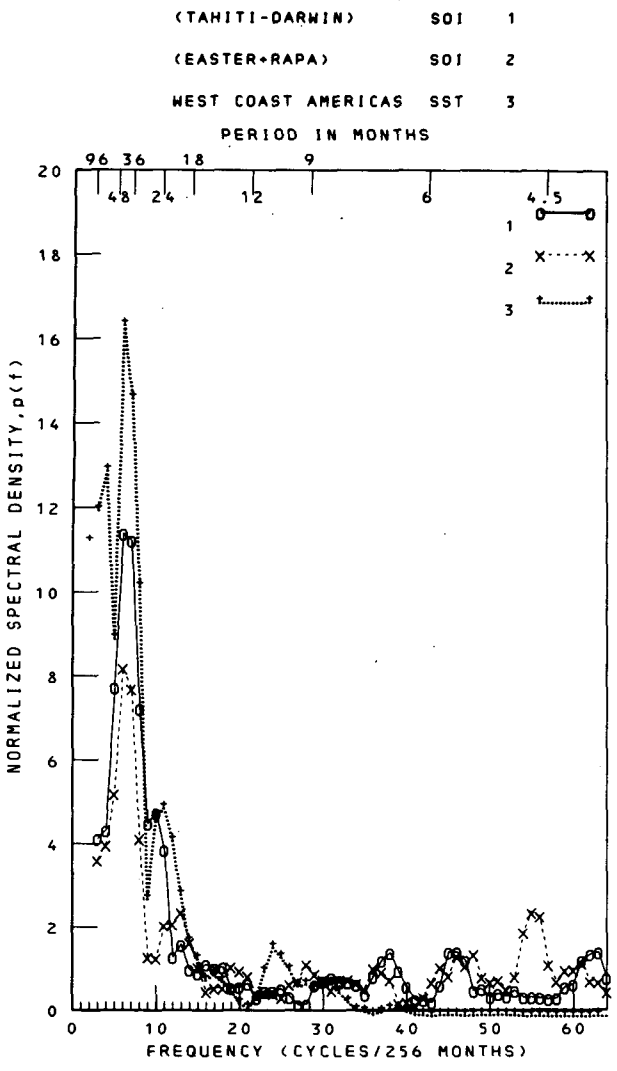

FIG. 2. Spectra for mean monthly anomaly time series (September 1953–December 1974) for Tahiti minus Darwin normalized surface pressure difference $(T - D)_N$, Easter Island plus Rapa surface pressure (E + R), and SST(1). See text.

the SST variance is found in sub-annual frequencies. The use of area-averaged SST anomalies also suppresses small-scale variability found in station or point data. The result is an SST index which shows a significantly stronger response in the SO frequency range than either of the pressure indices.

The coherence square and phase difference between $(T - D)_N$ and SST(1) are shown in Fig. 3. Values of coherence square exceed 0.9 in the SO frequency range (spectral estimates six and seven), higher than those between the two pressure indices (not shown). Changes in SST(1) lead opposite changes of $(T - D)_N$ by ~30°. For the average of spectral estimates six and seven (39.7 months) this is equivalent to a lead of 3.3 ± 0.3 months (95% significance). SST(1) lags opposite changes in (E + R) by about one month. Thus, the SST and station pressure data are highly coherent in the SO frequency range, and exhibit significant lag relationships.

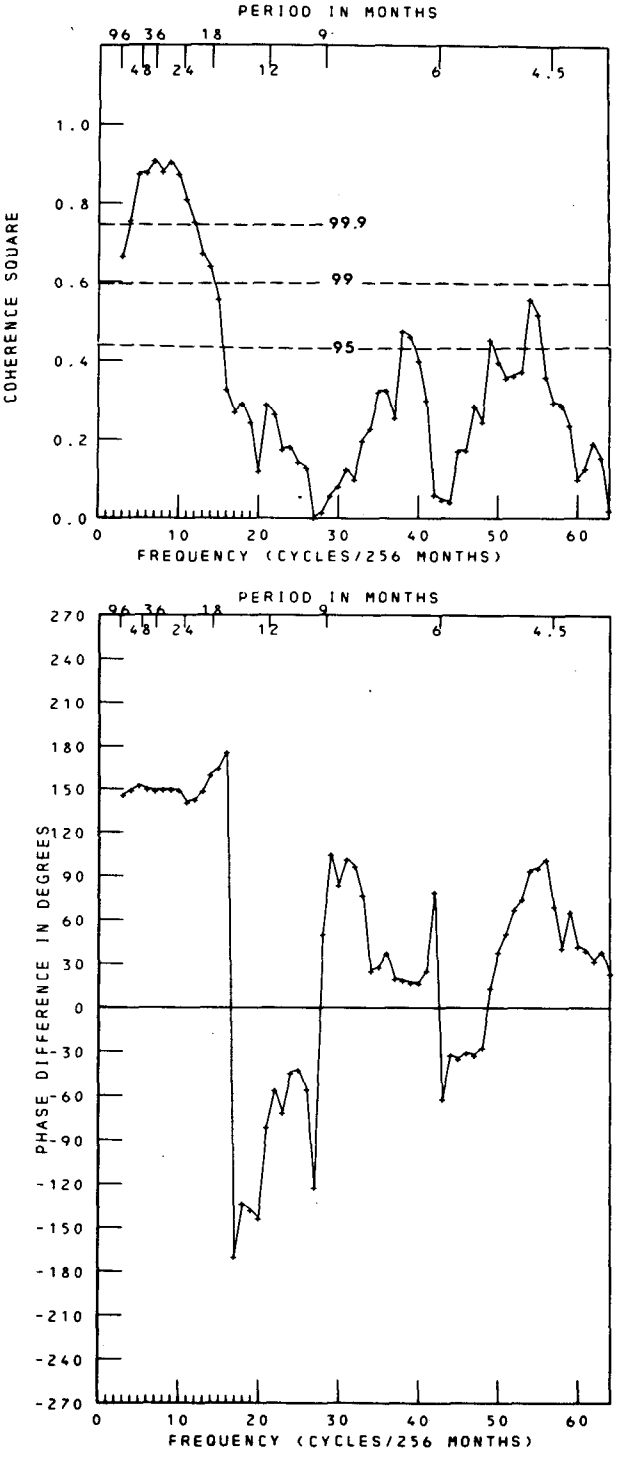

FIG. 3. Coherence square and phase, $(T - D)_N$ and SST(1). $(T - D)_N$ leads for positive values of phase. 95, 99 and 99.9% levels of significance (12.2 DF) are indicated for coherence square.

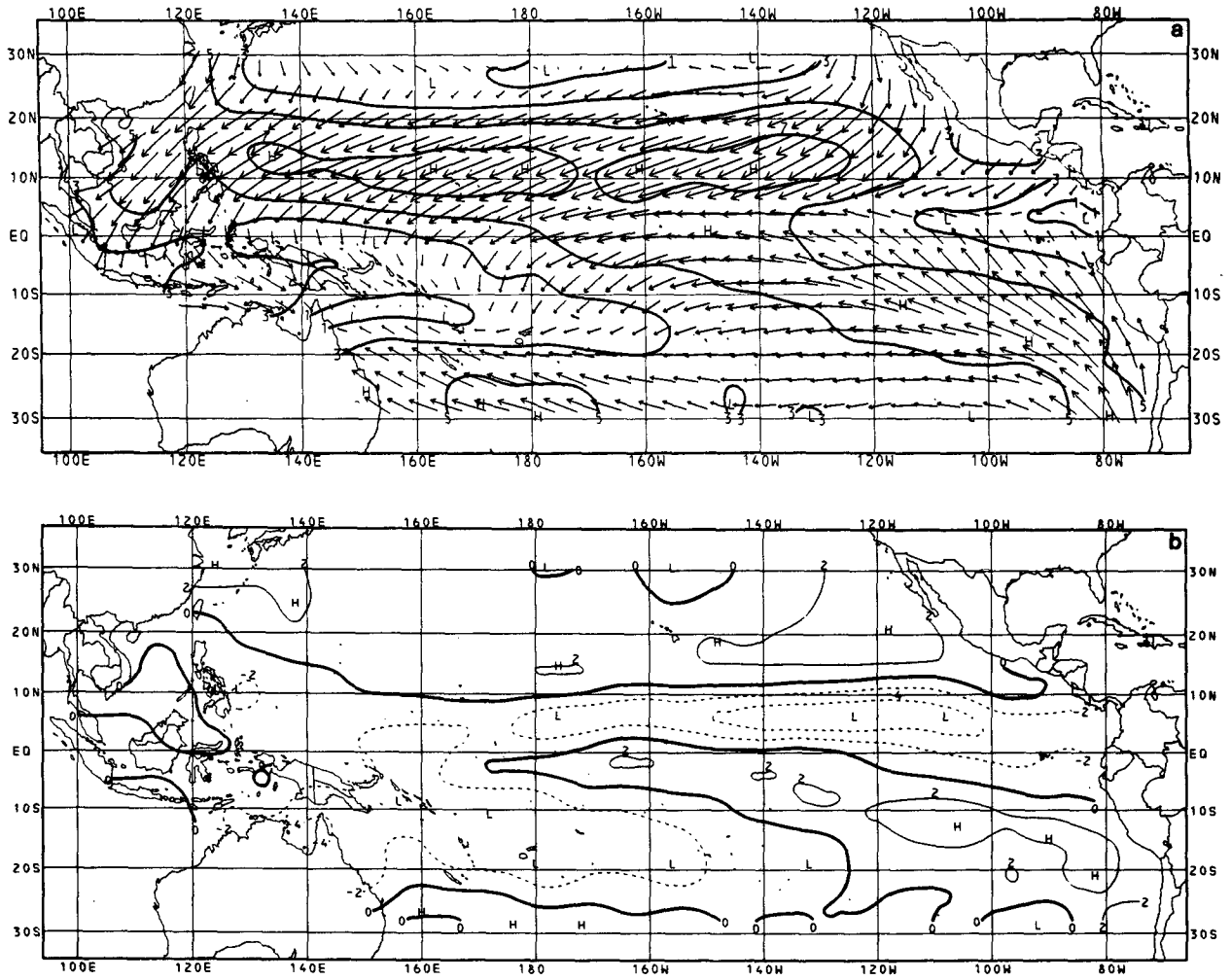

FIG. 4. Mean surface wind field and velocity divergence for February. Units of isotachs are m s^{-1}; units of divergence 10^{-6} s^{-1} (solid lines positive, dashed lines negative).

4. Ship track analysis

The results in this section are derived from an analysis of observations taken between 20°N–20°S along the six ship tracks shown on Fig. 1. Track 1 parallels the Central and South American Coasts, Track 2 extends southwestward from Panama, crossing the equator near the Galapagos Islands, and Track 3 extends from Panama to Tahiti. Track 4 crosses the equator between 140–145°W, while Tracks 5 and 6 cross the equator near Christmas Island, and Canton Island, respectively. North of 7°N, Tracks 1, 2, and 3 coincide.

a. Seasonal cycle

The general features of the tropical Pacific seasonal cycle have previously been described, e.g. Wyrtki (1964, 1965), Ramage (1975), Hickey (1975) and Wyrtki and Meyers (1976). Our new marine data base allows a somewhat more detailed description of the seasonal cycle of SST and surface winds. The following description is based on Figs. 4 and 5 which show the monthly mean (1949–76) surface wind and divergence fields over the area 30°N–30°S for the months of February and August.

In February (Fig. 4) the Northeast Trades extend westward across the North Pacific, merging in the western Pacific with the northeast flow of the Asian Winter Monsoon. Maximum tradewind speeds are ~7–8 m s^{-1}. The ITCZ in the eastern Pacific is located a few degrees north of the equator, and is associated with a wind speed minimum, as well as confluence and convergence in the surface wind field.

In the Southern Hemisphere, the Southeast Trades are interrupted by the SPCZ, which extends southeastward from the area of the Solomon Islands (Sadler, 1969). The SPCZ is marked by cyclonic flow, convergence, confluence, and a speed minimum. The austral summer ITCZ extends eastward from the

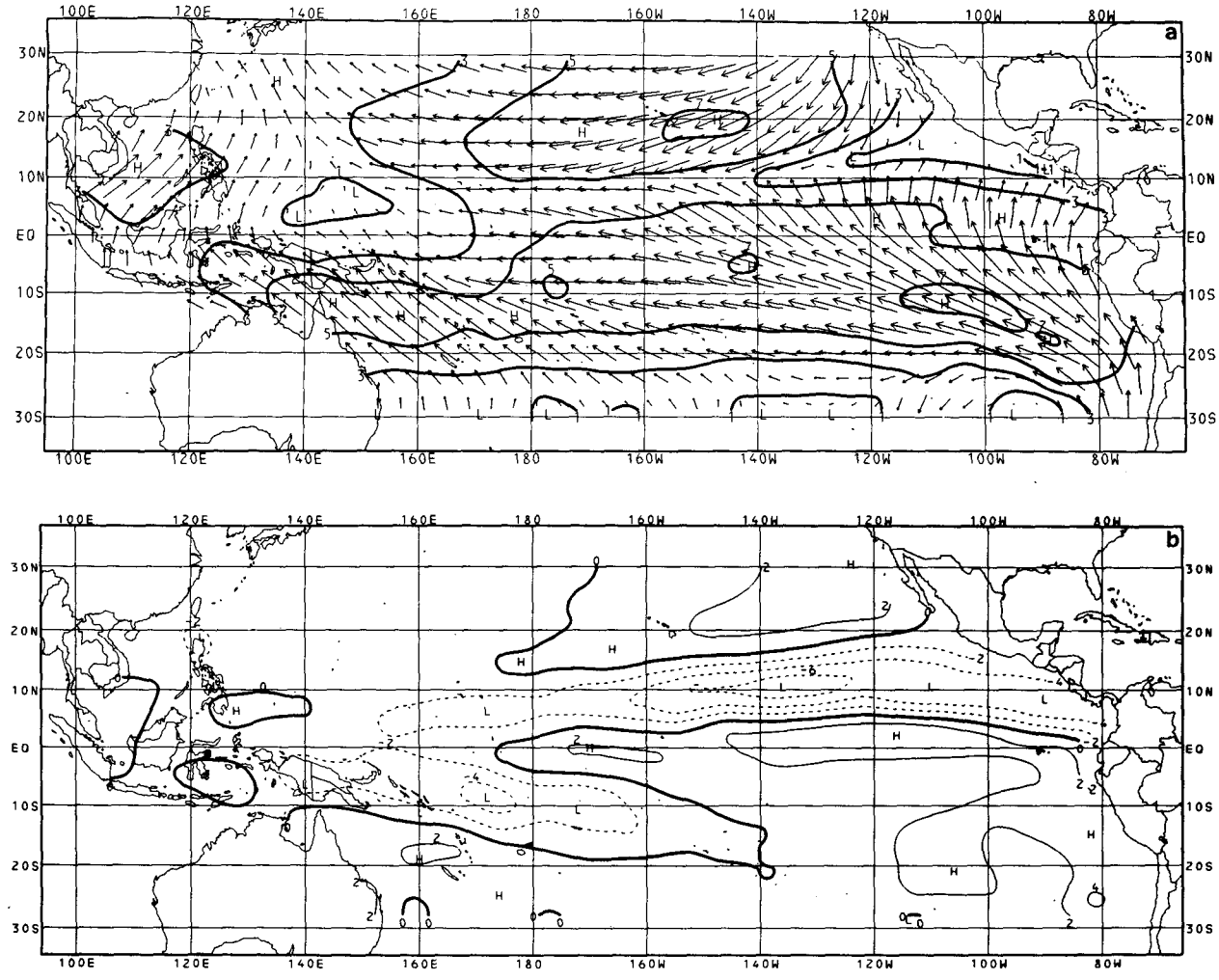

FIG. 5. Mean surface wind field and velocity divergence for August. Units as in Fig. 4.

Cape York Peninsula of Australia, and merges with the SPCZ.

In August (Fig. 5), the ITCZ and the Northeast Trades are shifted several degrees northward. West of 160°E the flow is part of the Asian Summer Monsoon circulation. In the transition area 0–10°N, 130–170°E, the flow is quite weak and the sign of the zonal component can be changed by a relatively weak wind anomaly. This area appears to be of particular importance in the initiation of the El Niño event (see Sections 5 and 6). In the Southern Hemisphere, the SPCZ is reflected in the surface divergence field, but the split in the South Pacific Trades, although still present, is less pronounced than it was during the austral summer. Note also, that unlike the Northern Hemisphere ITCZ, the SPCZ shows only small seasonal changes in position.

Mean monthly values of SST and wind components were computed for the ship tracks from data covering the period 1921–38 and 1949–76. [See also Donguy and Henin (1980a) for analysis of Track 3 data.] A few features observed in the ship track data are worth noting as additional background for the later discussion of interannual variability. There is a systematic phase shift and westward decrease in amplitude of the annual SST cycle along the equator (Wyrtki, 1965). At the South American coast, the lowest mean monthly values of SST occur during August–September, i.e., approximately in-phase with the Southern Hemisphere seasonal cycle. Moving westward along the equator, the minimum values are found at progressively later months, occurring during February–March on Track 6 (Fig. 1). A smaller phase shift is found in the months of maximum SST, i.e., from March–April on Track 1 to June on Track 6. On the three western tracks (4, 5, and 6), the months of minimum SST on the equator coincide with the months of maximum easterly wind component.

There is a mean westerly wind component on the equator on Track 1 throughout the year. Further west, the flow exhibits a small mean easterly com-

ponent on Track 2 throughout the year, with the possible exception of October–November. Tracks 3–6 show easterlies on the equator throughout the year, increasing in speed toward the west to ~5–6 m s^{-1} on Tracks 4 and 5, then decreasing to ~4–5 m s^{-1} on Track 6. The seasonal variation in mean monthly values is generally less than 1.5 m s^{-1}, but assuming a simple square dependence of stress on wind speed, this represents a seasonal variation in the zonal stress component of 65–85%.

b. Warm episodes along the South American coast

To date, much of the time series information on the nature and occurrence of El Niño, e.g., Ramage (1975), Wyrtki (1975) and Quinn (1979), has been derived from SST observations taken at stations along the coast of Ecuador and Peru. Thus, it is quite important to compare the "typical" coastal station El Niño signature with that observed offshore along Track 1. It is encouraging to find that the El Niño event is broadly similar in the SST(1) (average SST for latitudes 4–12°S on Ship Track 1) and coastal station (Talara, Puerto Chicama) time series. All spectra show the same SO peak (Fig. 6), although SST(1) shows more variance at very long periods, and all pairs of time series exhibit high coherence square down to periods of a few months (Fig. 7). There is, however, an important difference in the detailed behavior of El Niño at the coast and along Track 1. This is illustrated in Fig. 8, which shows composite SST anomaly curves for six El Niño's. Since the warmings are rather closely tied to the seasonal cycle, no effort was made to superpose specific features of the individual events. Rather, the data from the six events are simply averaged by calendar month. The anomalies are departures from the 1949–76 mean values. Although there is little difference in timing, the initial anomaly peak apparently first occurs at the coast. After the peak, the coastal stations show a sharp fall, sometimes to near normal SST. This is usually followed by a second extremely sharp anomaly peak in December or January[2]. This feature has been noted by Wyrtki (1975)

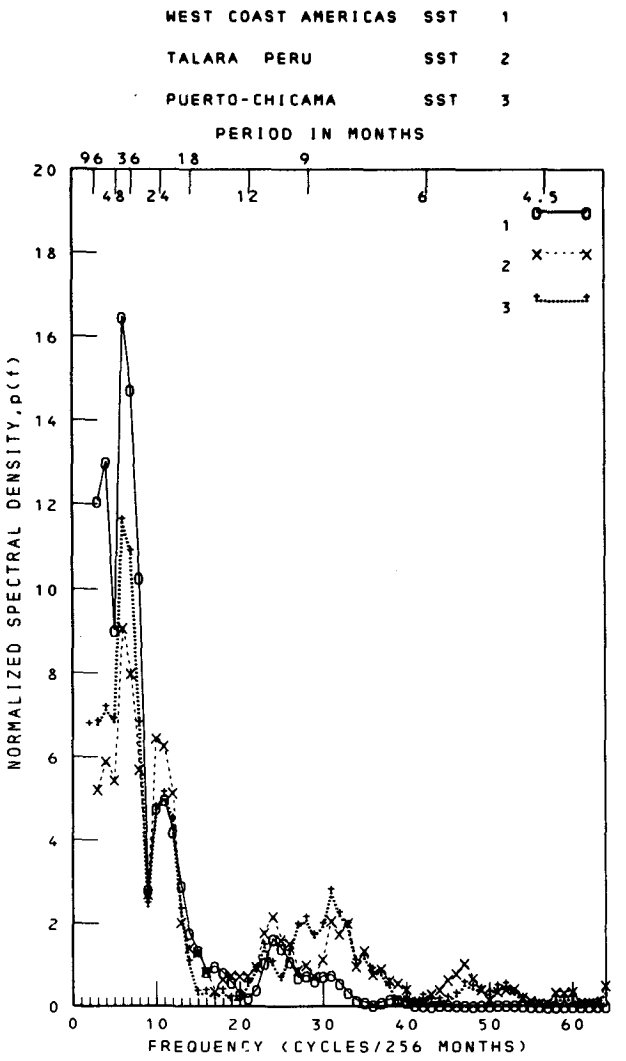

FIG. 6. SST anomaly spectra: (1) SST(1), (2) Puerto Chicama (7.7°S), (3) Talara (4.6°S). See text for definition of SST(1).

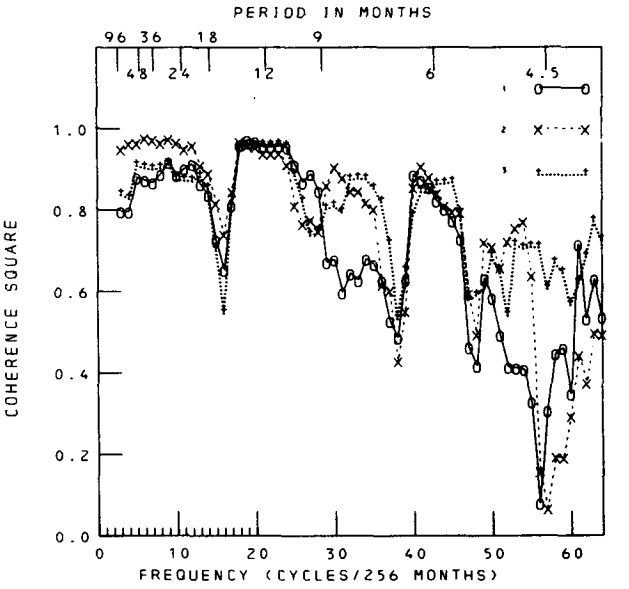

FIG. 7. Coherence square between SST time series (mean seasonal cycle not removed). (1) SST(1) and Talara, (2) SST(1) and Puerto Chicama, (3) Talara and Puerto Chicama.

[2] The dip in the anomaly values of the coastal station composites during December–January prior to the major rise appears to be an artifact resulting from the use of data from El Niño years in computing the long-term mean monthly values. Since the El Niño event is tied to the seasonal cycle, the peak SST anomalies tend to occur in the same calendar months. These months do not exhibit comparably large offsetting negative anomalies during non-El

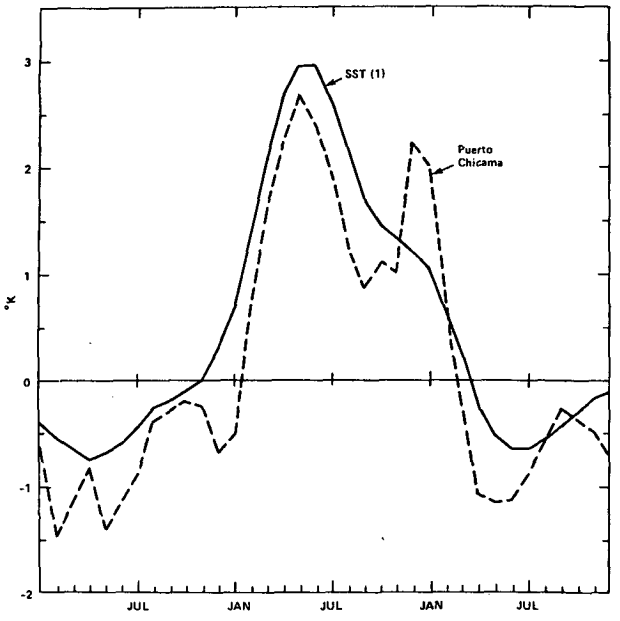

FIG. 8. El Niño SST anomaly composites: SST(1), Puerto Chicama. Composites are for six warm episodes (1951, 1953, 1957, 1965, 1969, 1972).

and others. In the case of SST(1), the initial anomaly decrease is rather less pronounced and is normally followed by a hesitation in the falling trend, or a minor upswing before a resumption of the falling trend. This difference between Track 1 and the coastal stations can hardly be due to the very slight amount of smoothing introduced by the filtering of the ship track data (Section 2). There is evidence of a similar but weaker pattern on Tracks 2 and 3. A single rather flat maximum generally appears on the three western tracks (Fig. 9). Ramage (1975) noted that the double peak does not appear in the Canton Island SST data.

A general picture of the warm episode along Ship Track 1 can be obtained from the six-event composite illustrated in Fig. 9. Maximum SST anomalies are found near 8°S during May–June, but because of the mean seasonal cycle, maximum SST's generally occur one to three months earlier. As the latitude separation from 8°S increases, the maximum anomaly occurs at progressively later dates, appearing at 20°S around September and at 20°N around the end of the year. Anomaly minima appear around 8°S approximately one year before and after the maximum, but their magnitude (1.2°C) is roughly half that of the maximum (2.8°C).

Enfield (1981a, 1981b) has examined the wind data from Peruvian coastal stations. He found that variations, on all time scales from diurnal to interannual, are primarily a response to local land–sea thermal forcing. On the interannual time scale, SST anomalies are positively correlated with enhanced southeasterly flow at Lima. Further north at Talara, in the area of enhanced El Niño rainfall, the southeast flow and SST anomalies are negatively correlated.

The coastal strip affected by land–sea forcing is ~100 km in width (Enfield, 1981a). The warm episode composite (Fig. 9) indicates enhanced southeast flow between 8–15°S, and weak easterly to northeasterly anomalies between 0–8°S during the middle and latter stages of the anomaly maximum. These variations appear to be more representative of the coastal station data than of the large-scale variations in the Southeast Trades, discussed in Section 5. An examination of the distribution of observations along Track 1 indicates that most of the ship reports are within this zone. Thus, the Track 1 winds may primarily reflect the land–sea forcing variations, rather than variations in the Southeast Trades. This difference in behavior between the coastal zone winds and those further offshore obscures the interpretation of results when data from both wind regimes are averaged, e.g., Barnett (1977a).

The SST time series for the six individual events composited on Fig. 9, as well as the weaker event of 1963[3], are superimposed on Fig. 10.

A strong trend toward positive anomalies normally appears by the December or by the January preceding El Niño. Only during the relatively weak events of 1951 and 1963 was the onset of the rapid rise delayed until the early months of the El Niño year. The peak anomalies occur between April and June (except for the 1963 event, which peaked during August). The anomaly peak is followed by a period of rapid fall, which in some cases extended uninterrupted into the middle of the next year. During most events, including all strong warmings, the fall leveled out or anomalies even rose to a secondary peak around the end of the year. This was followed by a resumption of a rapid fall with anomaly minima reached between May and August of the following year. The 1957 case was different in that significant

Niño years. Consequently, anomalies during non-El Niño years, and in the initial stages of the warming event, tend to show a small negative dip during December–January, the months of the secondary El Niño peaks. Similarly the pre-and post-El Niño minima may be unduly accentuated simply because of the effect of the major El Niño maximum on the long term mean monthly values during April–June.

This points up the problem of proper definition of "mean" conditions from which to compute El Niño departures. As a simple experiment we recomputed mean monthly values of SST(1) excluding the six El Niño years. The new anomaly time series showed stronger El Niño peaks, as expected, and in addition much of the small "inverse" El Niño cycle appearing in SST(1) during non-El Niño years (Fig. 13), as for instance 1959–62, was removed.

[3] Although this event was relatively weak near the South American coast, it was comparable in strength to the other six events in the central equatorial Pacific.

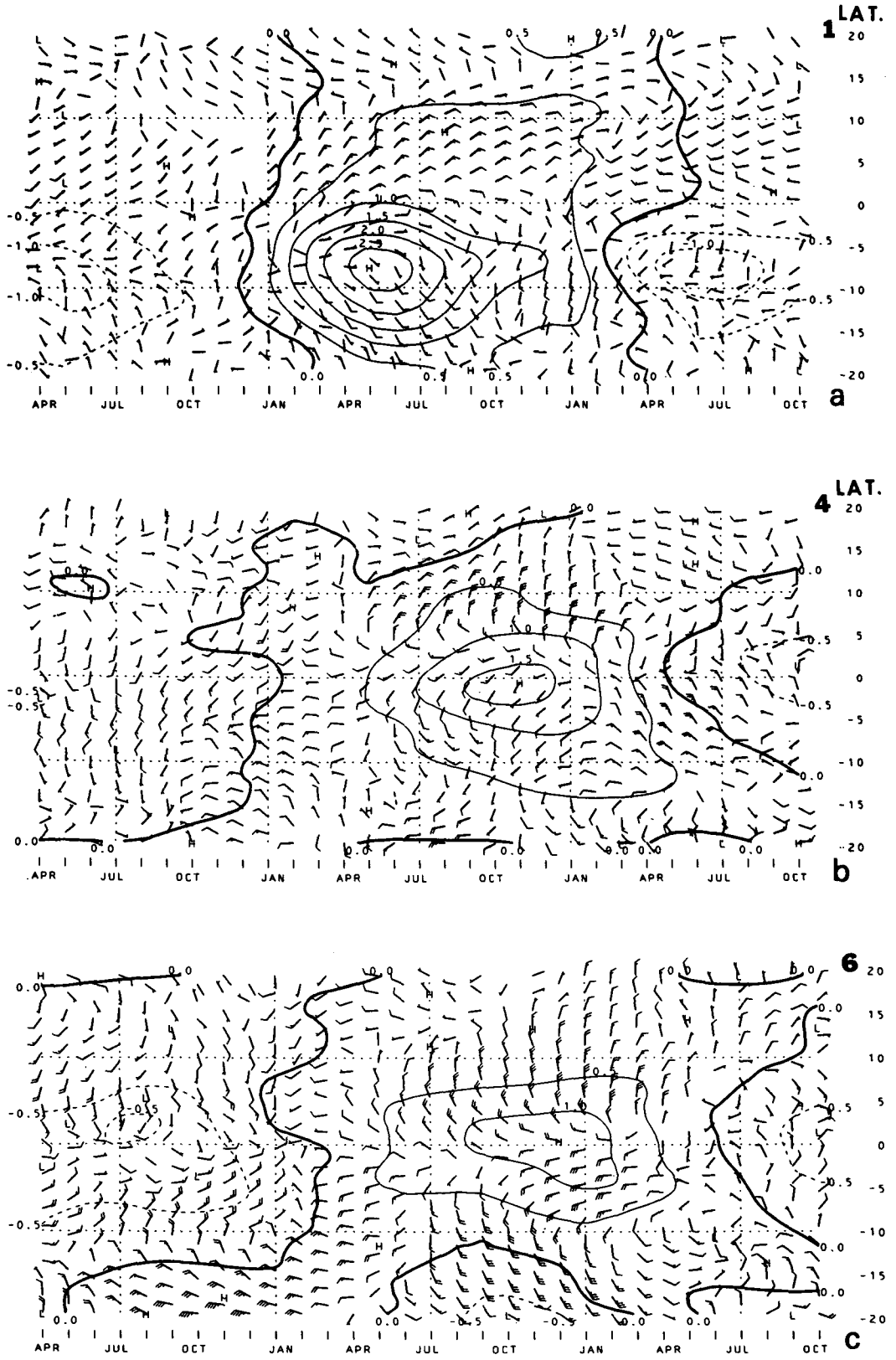

FIG. 9. Ship track composite wind and SST anomalies for six warm episodes (1951, 1953, 1957, 1965, 1972); Tracks 1 (a), 4 (b), and 6 (c). Full barb = 0.5 m s^{-1}. SST contours, °C.

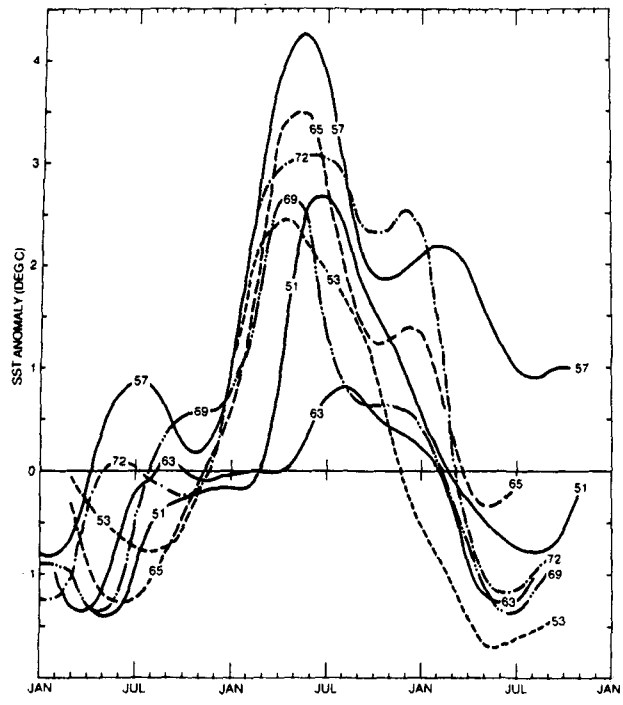

FIG. 10. SST(1) anomaly time series for the seven most significant warm episodes between 1950 and 73.

negative anomalies failed to reappear for several years following the warm episode. In this respect, the 1957 El Niño was similar to the 1976 event (Winston and Krueger, 1978; Krueger and Winston, 1979).

Warmings during the period 1921–38 (Fig. 11) were weaker, less frequent and exhibited less uniform behavior. Only one event, 1923, closely followed the pattern of events since 1949. The 1925–26 event was similar in many respects, but the relative strengths of the first and second peaks were reversed. The warming of 1932 peaked early (March), and the warming of 1930 was delayed, peaking in November.

c. SST and wind lag relationships

Previous investigators have presented evidence of a westward migration of SST anomalies which first appear along the Ecuador–Peru coast. Hickey (1975) showed evidence that year-to-year fluctuations in SST at Christmas Island and Canton Island lag those at the Galapagos by three and four months, respectively. Barnett (1977a) found evidence of a half-year lag between SST at Talara and Christmas Island. Quinn (1979) found maximum correlations at three to six month lags between SST at South American coastal stations and SST at Canton Island. Rasmusson and Carpenter (1980) reported preliminary results from ship track data which showed a westward migration of SST anomalies in the eastern equatorial Pacific. See also Weare (1982).

The time series of SST(1) and SST(6) are shown in Fig. 11. On the average, variations on Track 6 (Hawaii–Fiji) appear to lag those on Track 1 (West Coast of Americas) by several months. Table 1 shows SST lag correlations computed for Track 1 and cross-correlations between Track 1 and the other five tracks. It is apparent that the time lag of maximum correlation with SST(1) increases toward the west. There is a remarkable consistency in the data, the only exception being SST(5) which shows somewhat lower correlations than would be expected in light of the data from Tracks 4 and 6.

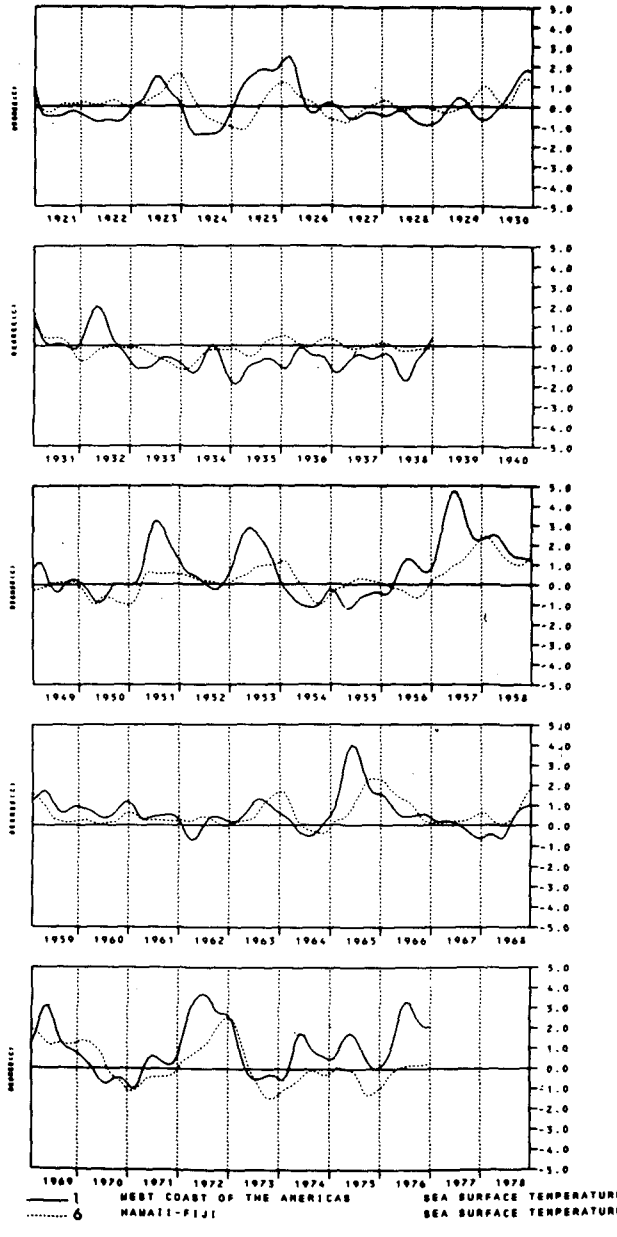

FIG. 11. Time series, SST(1), SST(6); 1921–38; 1950–76. See text.

SST anomaly spectra were computed for the six tracks for the period September 1953–December 1974. All spectra exhibit a sharply-defined SO peak

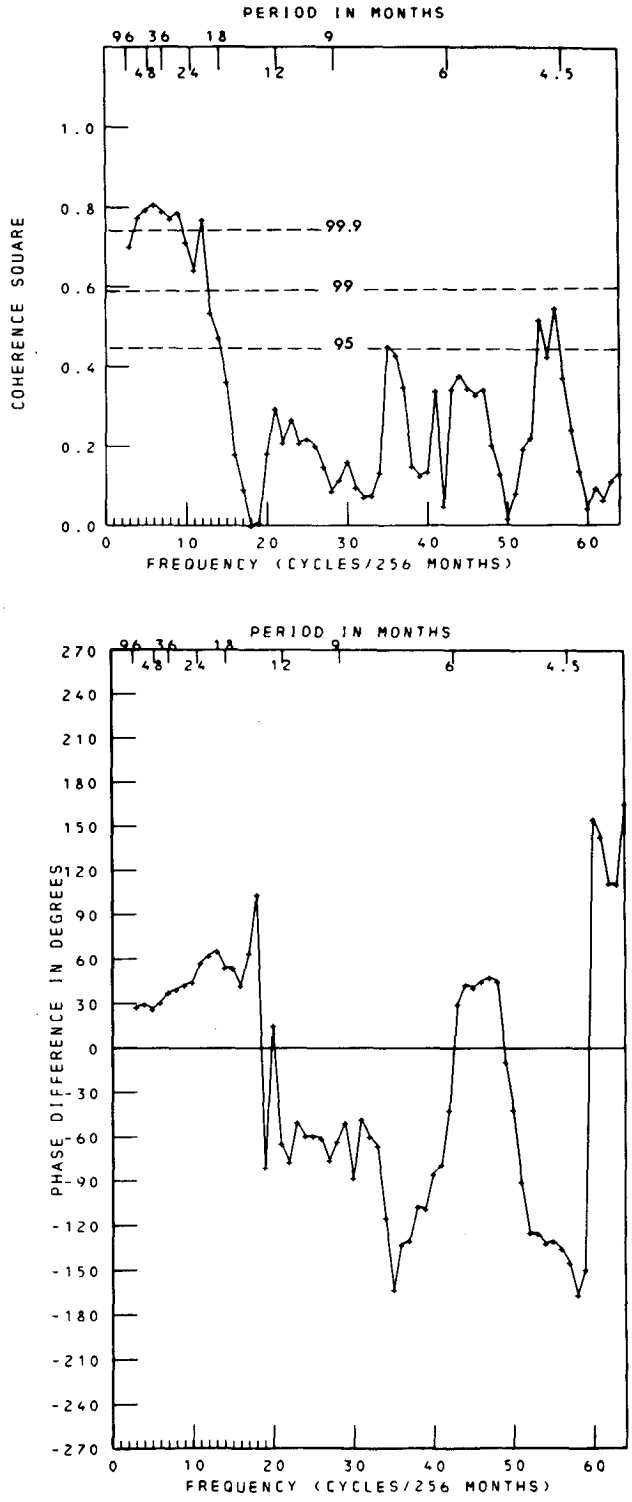

FIG. 12. Coherence square and phase, SST(1) and SST(6). SST(1) leads for positive values of phase.

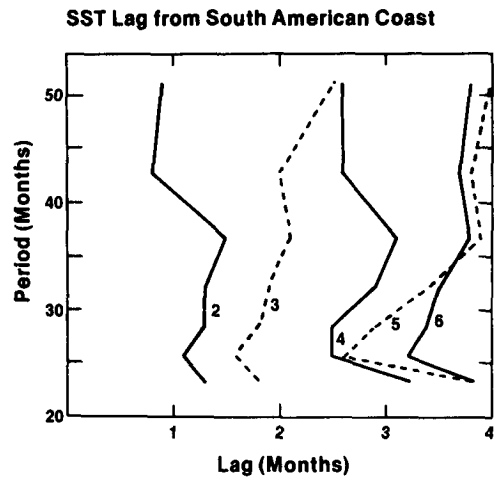

FIG. 13. Phase difference SST(1) and other tracks.

at spectral estimates six and seven (e.g., see Fig. 6). The spectra for the eastern tracks also exhibit a weak quasi-biennial maximum, a feature which is also found at the coastal stations (Fig. 6).

SST coherence square and phase angle were also computed for all pairs of tracks. High coherence square was found at the lower frequencies (e.g., Fig. 12). Fig. 13 shows the phase difference between Track 1 and the other five tracks for a range of periods which includes the SO. As in the case of the lag correlations (Table 1), the data show lags which increase toward the west. The only departure from the regular progression between tracks is again associated with SST(5) which shows roughly the same lag as SST(6) for periods longer than three years.

In summary, this analysis indicates that large-scale SST anomalies which appear off the coast of Peru tend to spread northwestward, then westward along the equator into the central Pacific, thus confirming the less comprehensive analyses of Hickey (1975), and Barnett (1977a), and quantitatively documenting the lag relationships. The lag between the Peru Coast and 170°W is typically three to six months. This represents an average speed of movement between 0.5 and 1.0 m s^{-1}.

Information on the relationship between eastern equatorial Pacific wind and SST variations during a warm episode can also be derived from the ship track data. The anomaly composites for the six warm episodes exhibit the following features (Fig. 9):

1) The positive SST anomaly on Track 1 is roughly twice the magnitude of the anomaly on the other tracks. The composites clearly show the westward migration of the eastern equatorial SST anomaly pattern.

2) On each track, the appearance of the positive SST anomaly is accompanied by the development of anomalous equatorward flow in both hemispheres.

TABLE 1. SST cross-correlations at various lags.

Cross-correlations between SST(1) and:	Lag (months)						
	0	1	2	3	4	5	6
SST(1) (W. Coast of S. America)	1.00	0.96	0.85	0.71	0.57	0.45	0.35
SST(2) (Panama-Galapagos)	0.88	0.89	0.84	0.76	0.65	0.54	0.43
SST(3) (Panama-Tahiti)	0.77	0.80	0.79	0.75	0.65	0.54	0.43
SST(4) (San Francisco-Tahiti)	0.57	0.63	0.66	0.66	0.65	0.61	0.56
SST(5) (Los Angeles-Christmas)	0.47	0.50	0.52	0.52	0.52	0.50	0.48
SST(6) (Hawaii-Fiji)	0.53	0.59	0.63	0.65	0.65	0.64	0.61

Conversely, the decay of the anomaly and subsequent reappearance of negative SST anomalies is accompanied by the disappearance of the equatorward flow anomaly.

3) Table 2 shows the percent of U and SST variance in the SO frequency band (spectral estimates six and seven) as well as the coherence square between the parameters, for the eight-degree latitude strip of maximum SST variability (Fig. 1). Phase differences are also shown, with R indicating that the difference is for out-of-phase variations. Except for Track 1, none of these phase differences reach the 95% significance level. Thus, on the three eastern tracks, the U and SST variations are essentially out-of-phase, and the U variance in the SO frequency band is relatively small. On the three western tracks, SST and U are essentially in phase with the percent of U variance in the SO frequency band increasing toward the west. Considering the westward migration of the SST anomaly pattern, and the in-phase relationship between U and SST on the three western tracks, it is apparent why Barnett (1977a) found that SST changes at Christmas Island were consistent with both local upwelling and advection mechanisms on the equator.

The time series for the heavily sampled shipping lanes provide the most detailed description of the interannual variability of SST and surface winds over the tropical Pacific. However, the six ship tracks provide no information west of the dateline, and east of the dateline they provide an incomplete picture of the development and spatial relationship of the two fields. A more complete spatial, but less detailed local picture of the evolution of the two fields during a warm episode is provided by the composites which are discussed in the next section. Finally, the results summarized in this section are placed in a broader context in Section 6b.

TABLE 2. Percent of total variance, coherence square, and phase difference for mean monthly U and SST in the SO spectral band (spectral estimates six and seven). The values are for the eight degree latitude strip of maximum SST variability (Fig. 1). The coherence square is the higher of the two spectral estimates. The phase difference is for SST leading, with R indicating that the difference is for out-of-phase variations. The 95% confidence limits are indicated for the phase differences.

Ship track	Percent of total variance in spectral estimates 6 and 7		Spectral estimate of maximum Coh^2 (SST, U)	Coh^2 (SST, U)	Phase difference (months) and 95% significance limits
	SST	U			
1	24.3	9.6	7 (36.6 mo.)	0.58	+2.8 ± 2.7 (R)
2	22.6	9.0	7	0.54	+1.4 ± 2.4 (R)
3	29.4	14.7	7	0.38	−0.4 ± 3.7 (R)
4	29.1	11.1	6 (42.7 mo.)	0.56	−2.0 ± 2.7
5	20.9	16.3	6	0.72	−0.9 ± 1.9
6	26.7	18.0	6	0.79	+0.0 ± 1.7

5. Wind and SST composites: 30°N–30°S

The scarcity of marine data over large portions of the tropical Pacific (Fig. 14) precludes the routine construction of reliable monthly anomaly maps. It is hoped that this situation can be improved in the future through the use of satellite data (Sadler and Kilonsky, 1981).

Compositing represents an attractive alternate approach to the study of a specific type of event. When used with care, compositing can serve as a powerful tool for uncovering features common to a number of individual cases. Initially, two types of composites were constructed for the area 30°N–30°S. For the first type, the superposed epoch method, various phases of each episode were identified and composited, e.g., onset of rapid rise along the Peru coast, anomaly maximum, and period of maximum fall. For the second type, the El Niño years were identified, and the data were simply averaged by calendar month, as was previously done with the ship track data. Although the timing of the warm episode varies somewhat (Fig. 10), the stronger events since 1949 have been remarkably well locked to the seasonal cycle. Consequently, the differences in the results from the two compositing schemes is minor. The results from the second method, which are presented in this section, can be viewed simply as the departure of the monthly mean "climatology" of the six warm episodes from the long-term climatology.

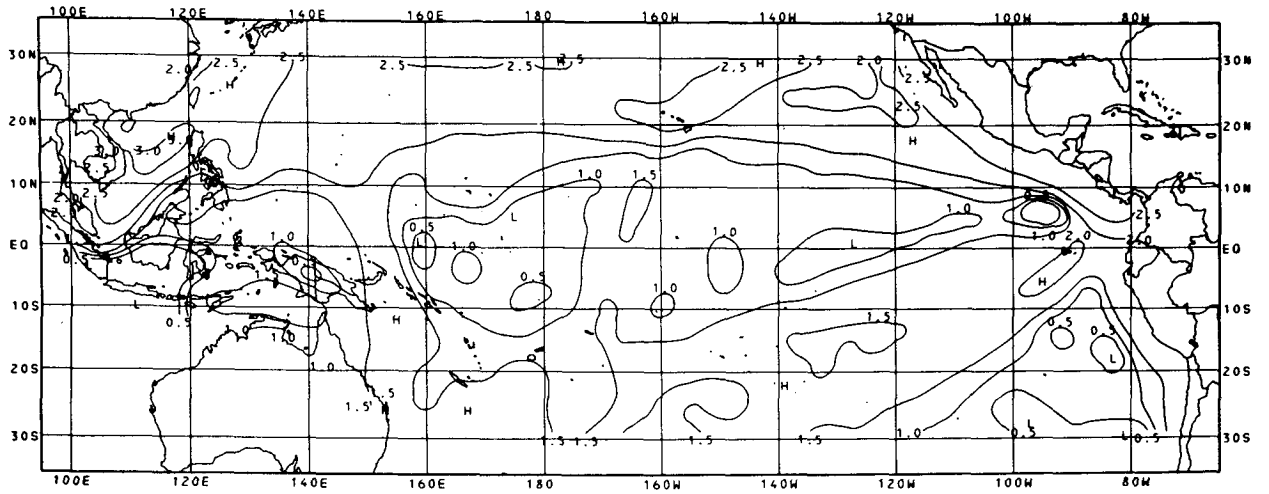

FIG. 14. Log of the average number of SST observations in each two-degree square used in each composite.

Composites were constructed for three-month averaged anomalies; thus each composite is the average of 18 individual monthly "maps". When data for a particular 2 × 2° square were not available for all 18 months, the composite value for that square was computed as the average of the available monthly values. If at least two months of data were not available, the square was marked missing. By far the greatest number of missing observations occurred during the first two warm episodes (1951, 1953). This, coupled with the relatively weak nature of these events, undoubtedly leads to composites which are most representative of the last four events (1957, 1965, 1969, 1972).

The distribution of data used in the composites is mapped on Fig. 14, in terms of the log of the average number of SST observations in each 2 × 2° square. The data density is quite uneven, ranging through two orders of magnitude. The equatorial region between ship tracks and the area between ship tracks west of Chile have the lowest number of observations. It is in these areas of poor data, and in regions where smaller-scale features may be distorted by smoothing, e.g., the anomaly wind field near the Peru coast, that the results are least reliable.

Objective analysis and smoothing are required to interpolate for missing values, and remove meaningless small-scale features resulting from the nonhomogeneous sampling. A standard NOAA computer system package was used for this purpose. Values for missing points were first obtained by linear interpolation in an east–west direction. This was followed by a two-dimensional smoothing, equivalent to a 7-point binomial smoother in the north–south direction and a 9-point smoother in the east–west direction. Due to equal weighting of data-rich and data-poor squares in the smoothing operation, these composites will generally be less reliable in the immediate vicinity of the ship tracks than the ship track composites themselves (Fig. 9).

Composites were constructed for the 33-month period beginning in April of the year preceding El Niño and ending in December of the year following El Niño. We shall present the three-month averaged composites centered on the following months: September(−1), December(−1), April(0), September(0) and January(+1), where the index refers to the year before(−1), during (0), or after (+1) El Niño. September(−1) is referred to as "Antecedent Conditions". December(−1) represents an early stage of the warm episode, when composite anomalies along the Peru Coast are near zero, but increasing rapidly. This is called the "Onset Phase". April(0) reflects conditions near or just before the time of maximum anomalies along the Ecuador-Peru coast, and is called the "Peak Phase". September(0) marks the end of the first sharp decrease of anomalies along the coast (Fig. 10). At this time, the anomaly maximum is beginning its westward shift from the coastal area into the central equatorial Pacific. This composite is referred to as the "Transition Phase". By January(+1), composite SST anomalies are again falling rapidly along the coast, and approaching normal values. In the central Pacific SST anomalies are past their peak but still large. We named this composite the "Mature Stage".

In the discussion which follows, reference will be made to Fig. 15 which shows the composite pressure anomalies for Easter Island, Darwin, and Rapa minus Tahiti. Fig. 16, which shows composite precipitation indices for the Line Islands (Washington, Fanning, and Christmas Islands) and the combination of Nauru (0.5°S, 167.0°E) and Ocean Island (0.9°S, 169.6°E) will also be referred to frequently. The precipitation index is the percentile rank or accumulated percentage frequency, i.e., the ratio of the

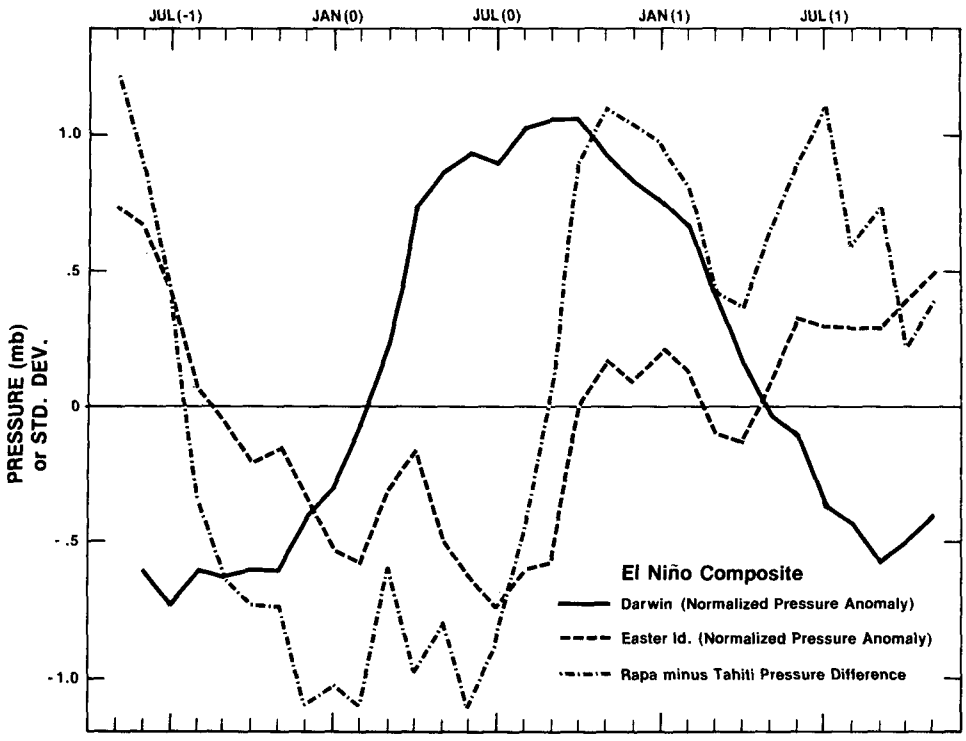

FIG. 15. Six-event composite of normalized pressure anomalies for Easter Island and Darwin, and Rapa minus Tahiti pressure gradient anomaly (mb). Values are three-month running means.

rank of the monthly precipitation amount in an ordered array to the total number of cases, expressed as a percentage and computed separately for each month (Meisner, 1976). The index anomaly is thus the percentage difference in rank from the median value.

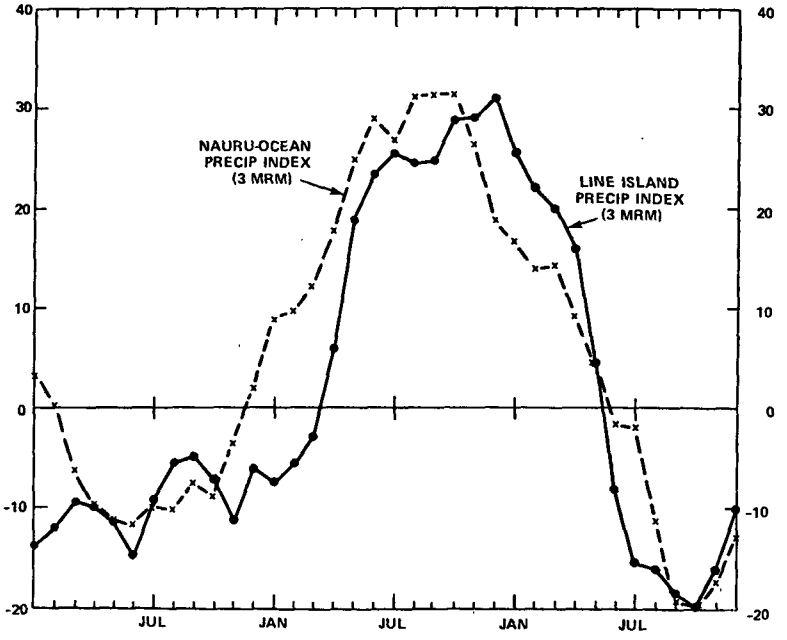

FIG. 16. Line Island and Nauru–Ocean Island precipitation indices. Values are three-month running means.

a. Antecedent conditions composite [September(−1)] (Fig. 17)

SST's along the Ecuador–Peru coast are below normal. However, the South Pacific high is weakening rapidly, as reflected by the negative trend in the surface pressure anomalies at Easter Island and Tahiti (Fig. 15). The pressure at Darwin remains well below normal, with no rising trend evident.

1) There is an intriguing area of small positive SST anomalies and northwesterly flow (weakened Southeast Trades) in the eastern Pacific south of 15°S. Particular caution must be exercised in interpreting the composites in this area of sparse data. The large spatial variations, and much of the month-to-month variability in this area undoubtedly arise from inadequate sampling. Nevertheless, when bulk averages for the poorly sampled area (14–20°S, 80–96°W; 20–30°S, 76–106°W) are computed, a consistent pattern of wind and SST variations emerges. Average southeasterly wind anomalies during April(−1)–August(−1) change to northwesterly anomalies in September(−1), increasing to ~0.8 m s^{-1} late in the year. This is qualitatively consistent with wind anomaly changes further west, and with the Rapa-minus-Tahiti pressure gradient anomaly (Fig. 16), which switches from positive to negative around August.

2) West of the dateline, there is enhanced easterly flow in the vicinity of the equator.

3) The major features of the southwestern Pacific anomaly fields appear to be organized about the normal September position of the SPCZ (NSPCZ), which is shown on the divergence composite. Specifically: a) SST anomalies are positive to the west and southwest of the NSPCZ, and negative to the northeast. b) The surface wind anomaly field is anticyclonic over the NSPCZ, where the climatological mean flow is cyclonic. c) There is anomalous convergence to the southwest, and anomalous divergence to the northeast of the NSPCZ. On the total divergence composite (not shown) the axis of maximum convergence, i.e. the SPCZ, is shifted slightly southwest of its normal position (NSPCZ). d) The Southeast Trades are weaker than normal southwest of the NSPCZ. e) North and east of the NSPCZ, between 10°N–10°S, the easterly component is stronger than normal.

This picture is consistent with a SPCZ displaced southwest of its normal position. Trenberth (1976) described these conditions as follows: "When the SO is positive, the SPCZ lies south of its mean position, not only in the Pacific but also near Darwin, and may change intensity. This is in accord with the lower pressure over Australia and more rainfall over and south of Indonesia, eastern Australia, and in the New Hebrides–Fiji Islands area, but less rainfall along the equator east of 160°E."

4) The divergence anomaly composite field is consistent with Trenberth's description of the precipitation anomalies and SPCZ displacement. In the central equatorial Pacific, the Line Island and Ocean–Nauru precipitation indices show subnormal precipitation at this stage of the event.

b. The Onset Phase composite [December(−1)] (Fig. 18)

At this time SST's along the Ecuador-Peru coast are near normal but rising rapidly. Dramatic changes have taken place in the central and western Pacific. Notable features of the composite are:

1) The positive SST anomalies west of Chile now appear more significant. Although again in an area of marginal data, the credibility of this feature is strengthened by its broadscale continuity on a number of consecutive composites [October(−1) through February(0)]. The three-month averaged composites for adjacent months are not independent, but the period is of sufficient length to include two independent composites. The evidence for a northwest wind anomaly maximum over this area appears to be considerably weaker, although it is present in various forms on composites covering the period August(−1) to December(−1).

2) The wind composite shows a general pattern of westerly to northwesterly anomalous flow across most of the Pacific south of 10°S. In the eastern Pacific this reflects a diminution of the southeast trades which is consistent with a weakening of the high pressure ridge overlying the area, as reflected in the below-normal pressures at Rapa and Easter Island (Fig. 15).

3) The well-organized pattern of wind, SST, and divergence anomalies in the southwest Pacific has become more chaotic, although there is still anomalous anticyclonic flow over the NSPCZ. This suggests a return of the SPCZ to a near-normal position.

4) In the central and eastern equatorial Pacific, positive SST anomalies have disappeared from the Indonesian area, and a new area of positive anomalies has developed near the dateline. This anomaly area, which was just beginning to appear on the Antecedent Conditions composite, is clearly separate from the positive anomaly west of Chile.

5) This SST anomaly is associated with the dramatic switch from easterly to westerly wind anomalies west of the dateline, which took place between October and November. The positive SST anomalies may result from decreased upwelling associated with the weakened easterlies.

6) The Nauru–Ocean Island Precipitation Index (Fig. 16) indicates enhanced precipitation along the equator west of the dateline. East of the dateline, the

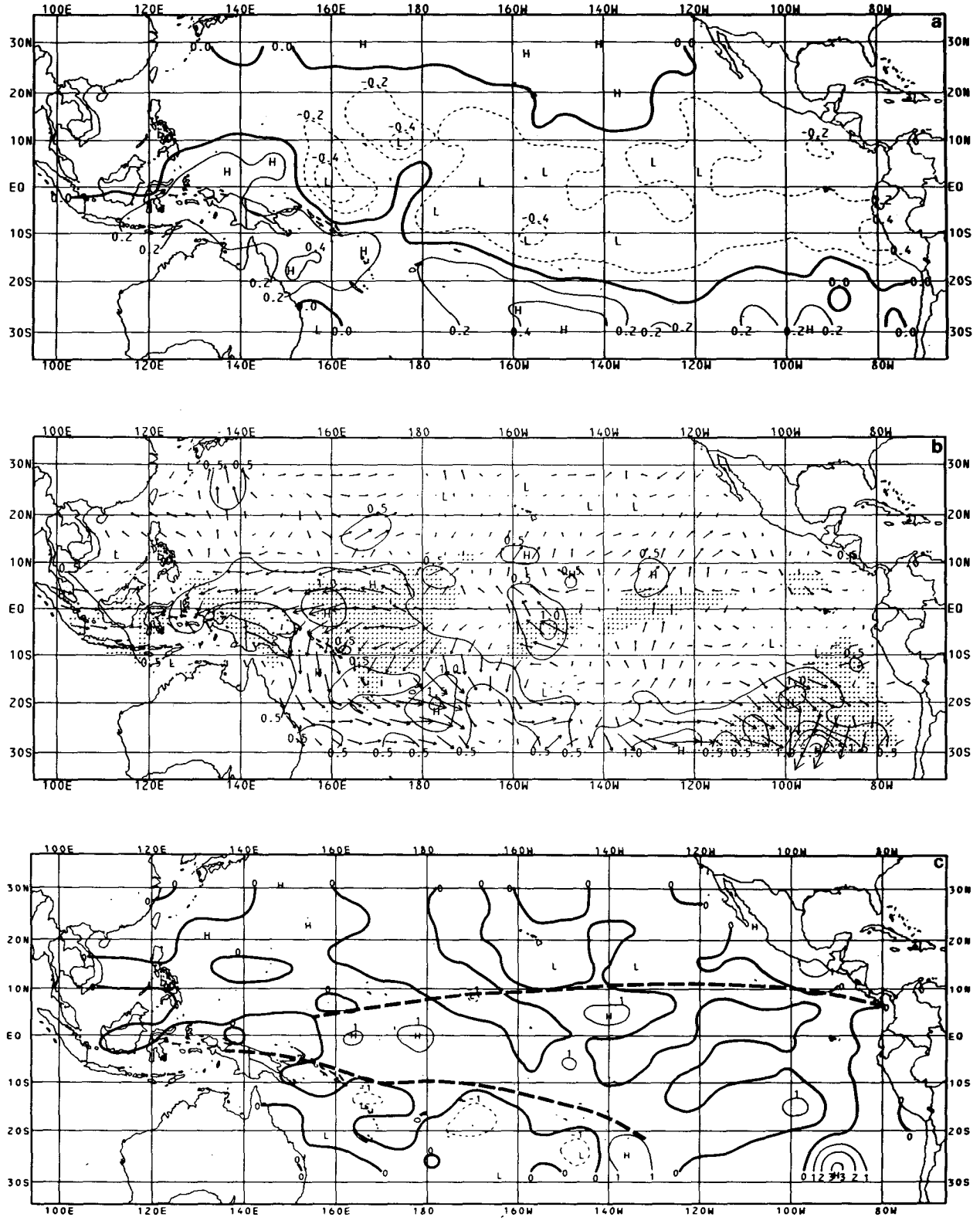

FIG. 17. Antecedent conditions anomaly composite (averages for August–October of the year preceding El Niño). (a) SST (°C), (b) wind anomaly (m s^{-1}), (c) velocity divergence (10^{-6} s^{-1}). The normal positions of the axes of convergence associated with the SPCZ and ITCZ are indicated on the convergence composite. Areas in which the number of observations averages less than 10 in a two-degree square are shaded on the wind composite.

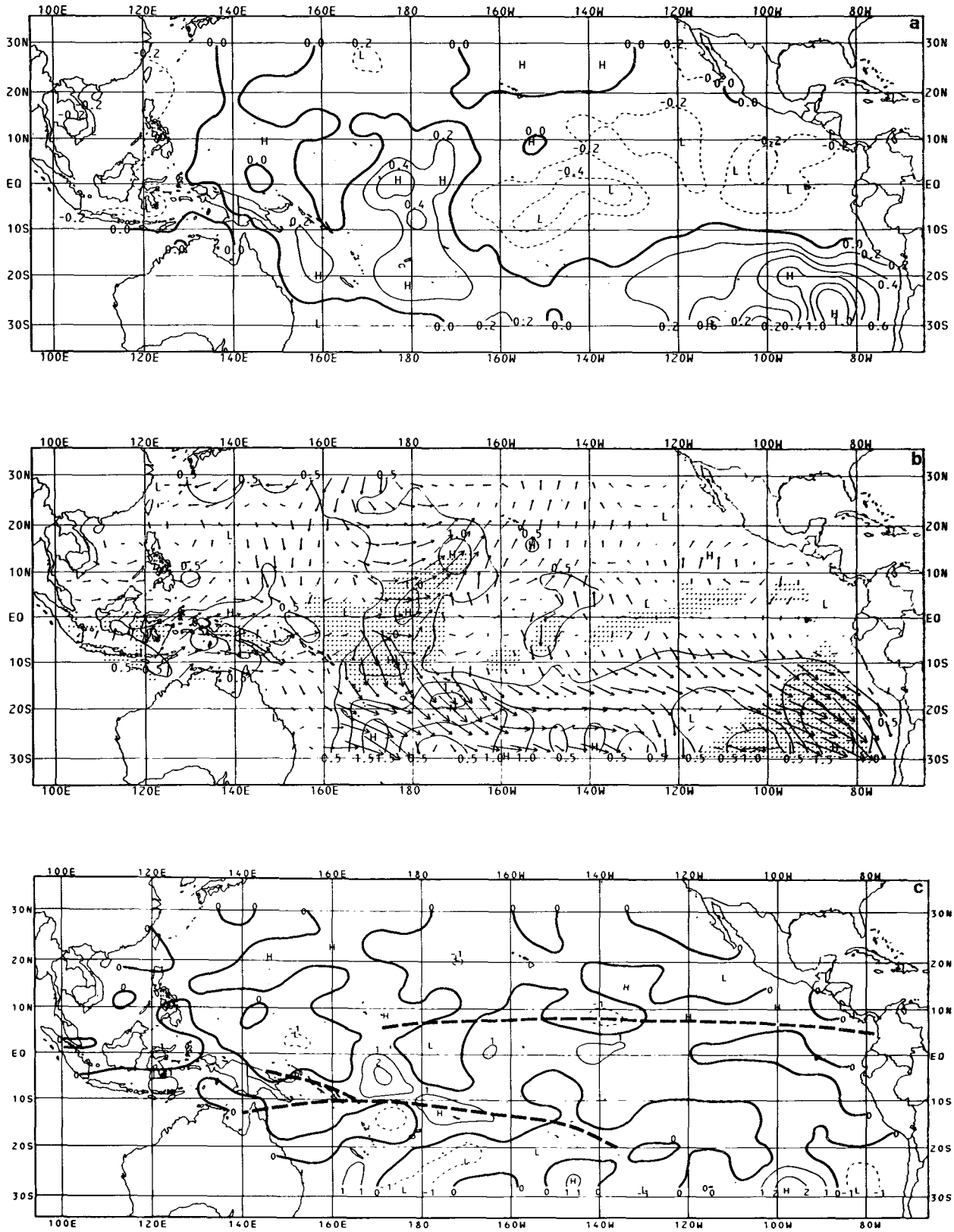

FIG. 18. Onset Phase anomaly composite. (Averages for November–January prior to maximum positive SST anomalies on Ecuador–Peru coast.) Units and shading are as in Fig. 17.

Line Island Index does not yet exhibit positive anomalies. The divergence anomaly composite exhibits a weak tendency for positive values near the equator east of the dateline, consistent with the Line Island Index, and a reflection of the weak poleward drift from near the equator which appears in both hemispheres on the wind composite. West of the dateline, the composite does not show the anomalous convergence expected in association with the positive Nauru–Ocean Island Precipitation Index anomaly. This may be due to inadequate sampling resulting from the small number of observations in this area.

c. *The Peak Phase composite [April(0)] (Fig. 19)*

An extensive area of positive SST anomalies now extends along the equator from the South American coast to 160°E. The positive SST anomaly near the dateline on the Onset Phase composite (Fig. 18) reached its greatest intensity in January, then spread both eastward and westward along the equator and weakened. It is now in the process of merging with the rapidly-developing positive anomaly area spreading westward from the South American coast. Other important features of the composites follow.

1) As the positive SST anomalies along the Ecuador–Peru coast increased in magnitude and area, the positive anomalies west of Chile diminished. The composites do not indicate a migration of anomalies from one area to the other, but rather suggest the decay and development of two separate anomaly areas.

2) The westward extension of positive anomalies along the equator is accompanied by the development of an anomalous northerly flow across the normal position of the ITCZ (NITCZ) between 110°W and 170°E. The associated belt of anomalous convergence south of the NITCZ is consistent with the reported southward shift of the ITCZ during the 1972 warm episode reported by Ramage (1975).

3) Precipitation anomalies in the central and eastern equatorial Pacific appear to be broadly consistent with this surface convergence anomaly. The data compiled by Taylor (1973) indicate a strong average enhancement of precipitation at San Cristobal in the Galapagos Islands during March, April, and May of El Niño years[4]. Further west, the Line Island Precipitation Index (Fig. 16) shows a strong increase, while anomaly values at Nauru–Ocean Island have also continued to increase. These scattered stations and the anomalous low-level convergence pattern suggest an enhancement of precipitation south of the NITCZ from near the South American coast westward to at least 165°E.

4) In the western and central Pacific the broad-scale wind and SST anomaly fields are evolving into a pattern quite different from that found on the Antecedent Conditions composite (Fig. 17). Negative SST anomalies now appear southwest of the NSPCZ, and positive anomalies to the northeast. Anomalous cyclonic flow now exists over and to the northeast of the NSPCZ. Enhanced southeast trades now appear east of Australia, and there is anomalous divergence southwest of the NSPCZ. These features are consistent with a SPCZ located slightly northeast of its normal position. Near the equator, the westerly anomalies which appeared just west of the dateline on the Onset Phase composite have spread eastward to ~160°W.

5) Coastal station data (Enfield, 1981a, 1981b) and data along Ship Track 1 show enhanced southeasterly flow along the lower Peru coast, as discussed in Section 4. The absence from the composite of this important smaller-scale feature is undoubtedly the result of smoothing.

d. *The transition phase composite [September(0)] (Fig. 20)*

Large positive SST anomalies now cover a vast area of the eastern and central equatorial Pacific. Near the South American coast the anomalies have diminished rapidly between June(0) and September(0). At the coastal stations, SST's often return to near-normal values during September(0)–October(0), prior to rising to a second positive anomaly peak in December(0)–January(+1) (Fig. 8). The SST anomaly maximum is no longer located near the coast, but is shifting into the central equatorial Pacific.

Other important features are:

1) The belt of anomalous northerly flow across the NITCZ has strengthened and expanded northward with the seasonal migration of the ITCZ. This anomaly feature is at peak strength during August–September. The same holds true for the belt of anomalous convergence south of the NITCZ. There is a weak southerly anomaly in the Southern Hemisphere near the equator between 90 and 140°W.

2) In the western equatorial Pacific, the wind anomaly pattern between 0 and 10°N shows a dramatic reversal from September of the previous year (Fig. 17). Westerly anomalies of more than 2 m s^{-1} now exist over much of this area, and actual westerly flow typically extends east of 160°E.

3) The precipitation index anomalies reflect the surface convergence in the central equatorial Pacific. Anomaly values at Nauru–Ocean Island (Fig. 16) are near their maximum. Anomalies at the Line Islands are also large, and increasing. In the Galapagos

[4] The San Cristobal rainfall data have been treated only in a qualitative manner. There was a break in the published record between 1961–63 after which Taylor's data suggest a change in the location or exposure of the gage.

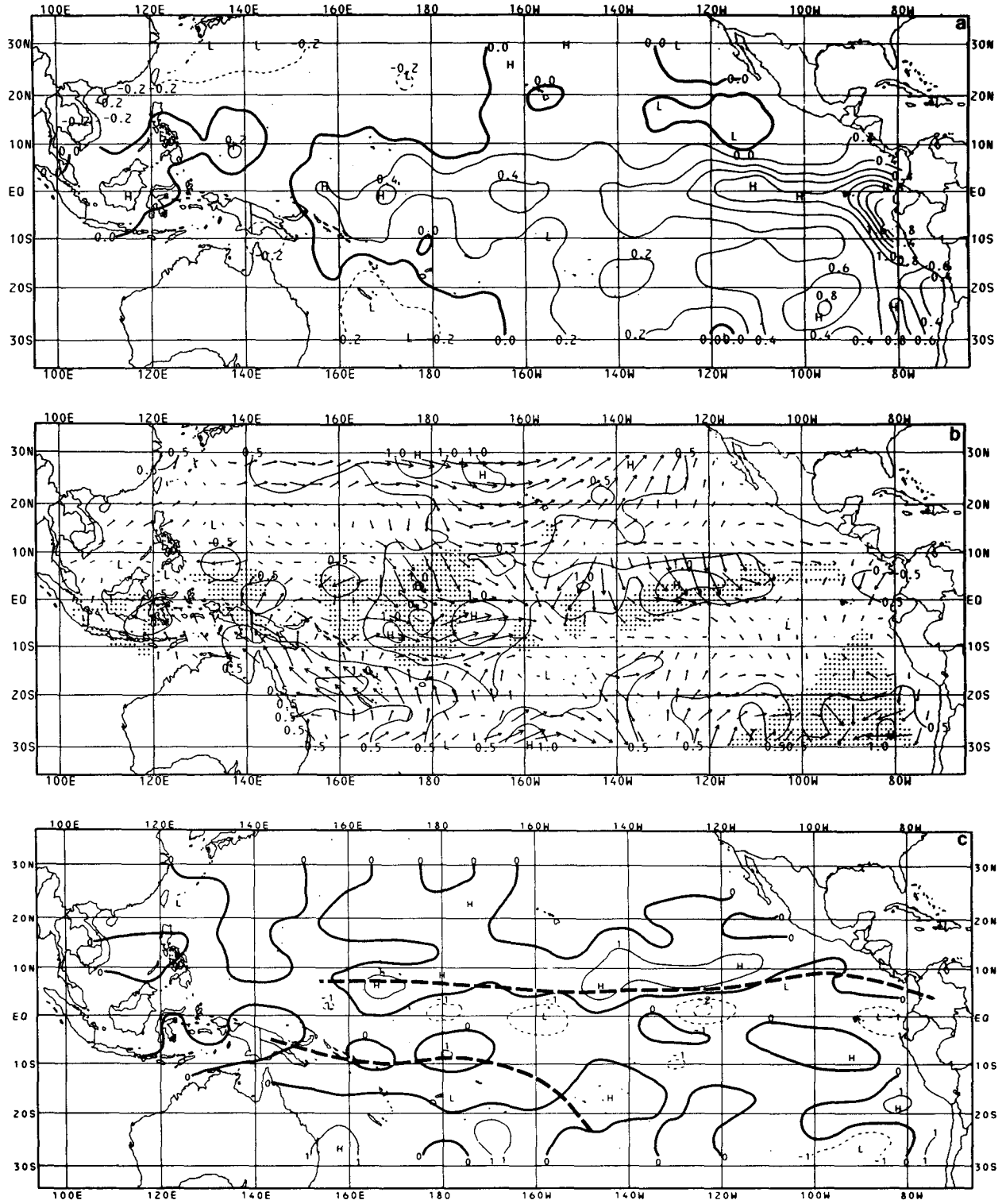

FIG. 19. Peak Phase composite. (Averages for March–May of El Niño year.) Units and shading are as in Fig. 17.

Islands, the precipitation anomalies peaked near the time of maximum SST anomalies, and have now diminished to small positive values.

4) The SST and wind anomaly fields in the southwest Pacific clearly reflect a northeast displacement of the SPCZ. Cyclonic anomalous flow appears over

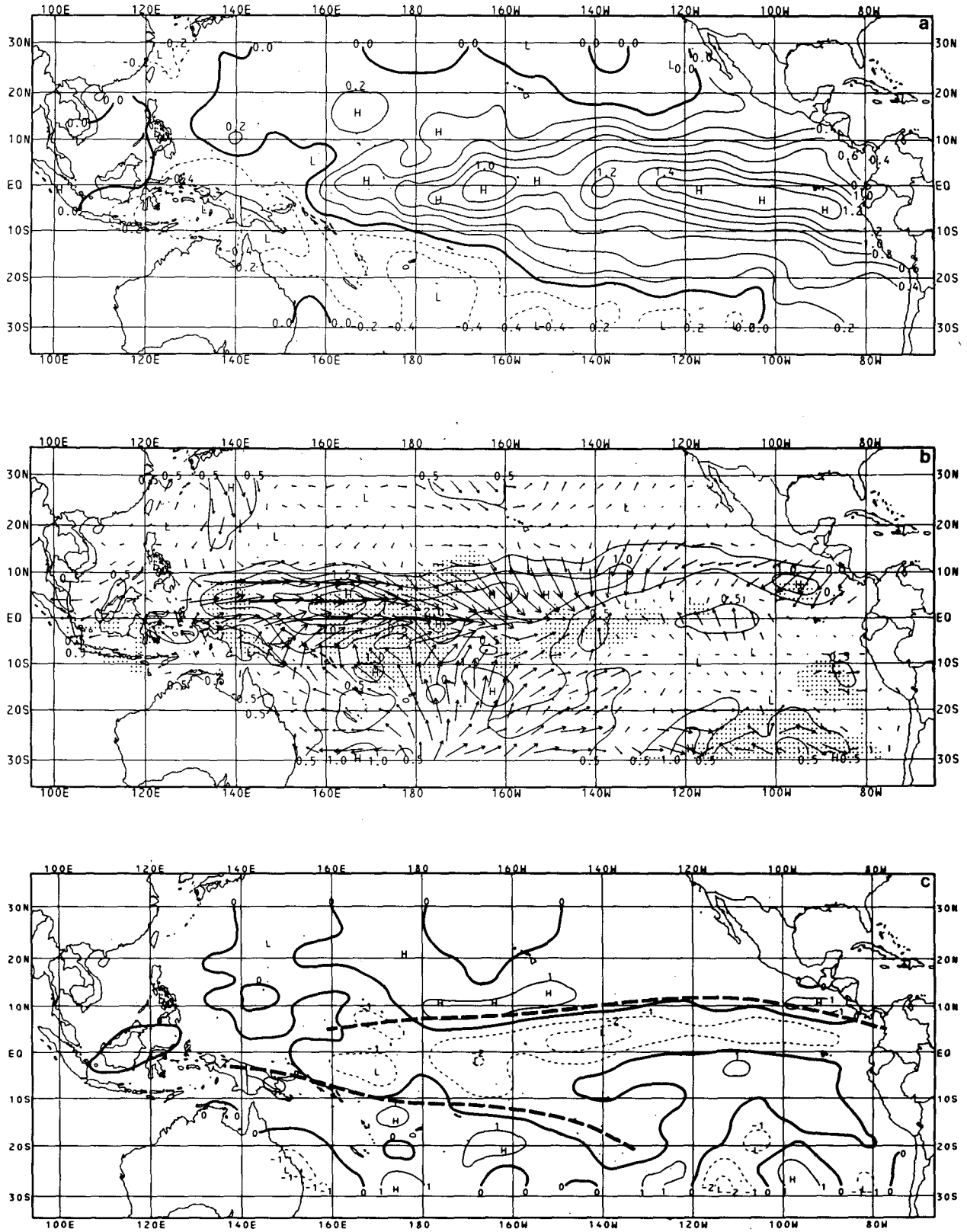

FIG. 20. Transition Phase anomaly composite (Averages for August–October of El Niño year). Units and shading are as in Fig. 17.

and to the northeast of the NSPCZ. Negative SST anomalies and anomalous divergence appear southwest of the NSPCZ, with anomalies of opposite sign to the northeast.

e. The Mature Phase composite [January(+1)] (Fig. 21)

This composite represents conditions at the time when teleconnections with the Northern Hemisphere extratropics are strongest. Positive SST anomalies continue to cover a huge region of the central and eastern equatorial Pacific, having reached peak values of between 1.5–2.0°C during November–December. SST's near the South American coast have returned to near normal.

Other composite features are:

1) The belt of anomalous northerly flow across the NITCZ has moved southward with the seasonal migration of the ITCZ, and has shifted westward, no longer appearing east of 110°W.

2) In the Southern Hemisphere, the anomalous flow associated with the northeastward displacement of the SPCZ exhibits a well-developed, coherent pattern, with pronounced cyclonic anomalous flow well to the northeast of the NSPCZ.

3) The shifting of the two major convergence zones results in a smaller wedge-shaped dry zone in the eastern tropical Pacific, and a concentration of the anomalous convergence in the central equatorial Pacific.

4) The precipitation anomaly pattern in the central Pacific implied by the divergence anomaly composite is consistent with the pattern shown in the EOF analysis of outgoing longwave radiation data by Heddinghaus and Krueger (1981). It is also consistent with the precipitation data from equatorial stations. Data from San Cristobal indicate only a weak enhancement of precipitation in the Galapagos Islands primarily associated with those warm episodes which exhibit a local secondary SST anomaly peak around the end of the year. The Nauru–Ocean Island Precipitation Index anomaly peaked several months earlier (Fig. 16), and the Line Island Precipitation Index anomaly is just past its peak.

5) In the western Pacific, there appears to be broad agreement between the composite divergence anomaly field and the observed precipitation anomaly pattern: a) The large-scale wind anomaly pattern over the northwestern Pacific reflects a weakened Northeast Monsoon circulation, and is associated with a large area of divergence extending eastward from the Philippines. b) In the southwest Pacific, the area of divergence extending eastward from Australia between 10–20°S is associated with weakened southeast tradewinds and diminished convergence in the southern summer ITCZ located in this area. c) A precipitation composite prepared by J. M. Wallace and J. D. Horel (pers. comm., 1981), using data compiled by Taylor (1973), agrees remarkably well with the divergence pattern in both the northwest and southwest Pacific. Their composite shows diminished rainfall in both areas during northern winters following El Niño. Donguy and Henin (1980b) obtained similar results for the southwestern Pacific. In addition, they found a positive correlation between precipitation deficiency in this area and the El Niño intensity index of Quinn *et al.* (1978). Pittock (1975) found a strong SO signal in eastern Australian rainfall, with lighter amounts during periods of low pressure over the eastern Pacific. The precipitation anomaly pattern in the western Pacific is also consistent with the EOF analysis of Heddinghaus and Krueger (1981).

6. Discussion and conclusions

A number of the more significant findings and conclusions from this study are summarized below.

a. Warm episode precursors

During July(−1)–October(−1), the most strongly developed and coherent anomaly fields are found over the western equatorial and southwest Pacific. The broadscale aspects of these anomaly fields appear to be associated with a southwest displacement of the SPCZ. This is typical of high SOI conditions (Trenberth, 1976), and is associated with below-normal surface pressure, above normal SST, diminished Southwest Tradewinds and enhanced surface convergence and precipitation in the western equatorial and western South Pacific. The opposite pattern of anomalies are found northeast of the SPCZ.

The relationship between variations in the surface wind field and warm episodes is a crucial element in El Niño theory. Model studies (Hurlburt *et al.*, 1976; McCreary, 1976) suggest that El Niño may be a dynamic response to remote rather than local atmospheric forcing. Based on case studies of the 1972 and 1976 El Niños, Wyrtki (1975, 1979b) identified an intensification and subsequent relaxation of the tradewinds in the central equatorial Pacific as the remote forcing mechanism. For further background and discussion of this theory, see Enfield (1980), O'Brien *et al.* (1980), and Philander (1981). The ship track data show no evidence of a decrease in the tradewinds in the central equatorial Pacific prior to the onset of warming along the Peru coast. However, an area of significant easterly wind anomalies appears west of the dateline on the July(−1)–October(−1) wind composites, and rapidly disappears after October(−1). Goldenberg and O'Brien (1981) show an extensive area of interannual variability in the zonal flow between 130°W and 130°E in the

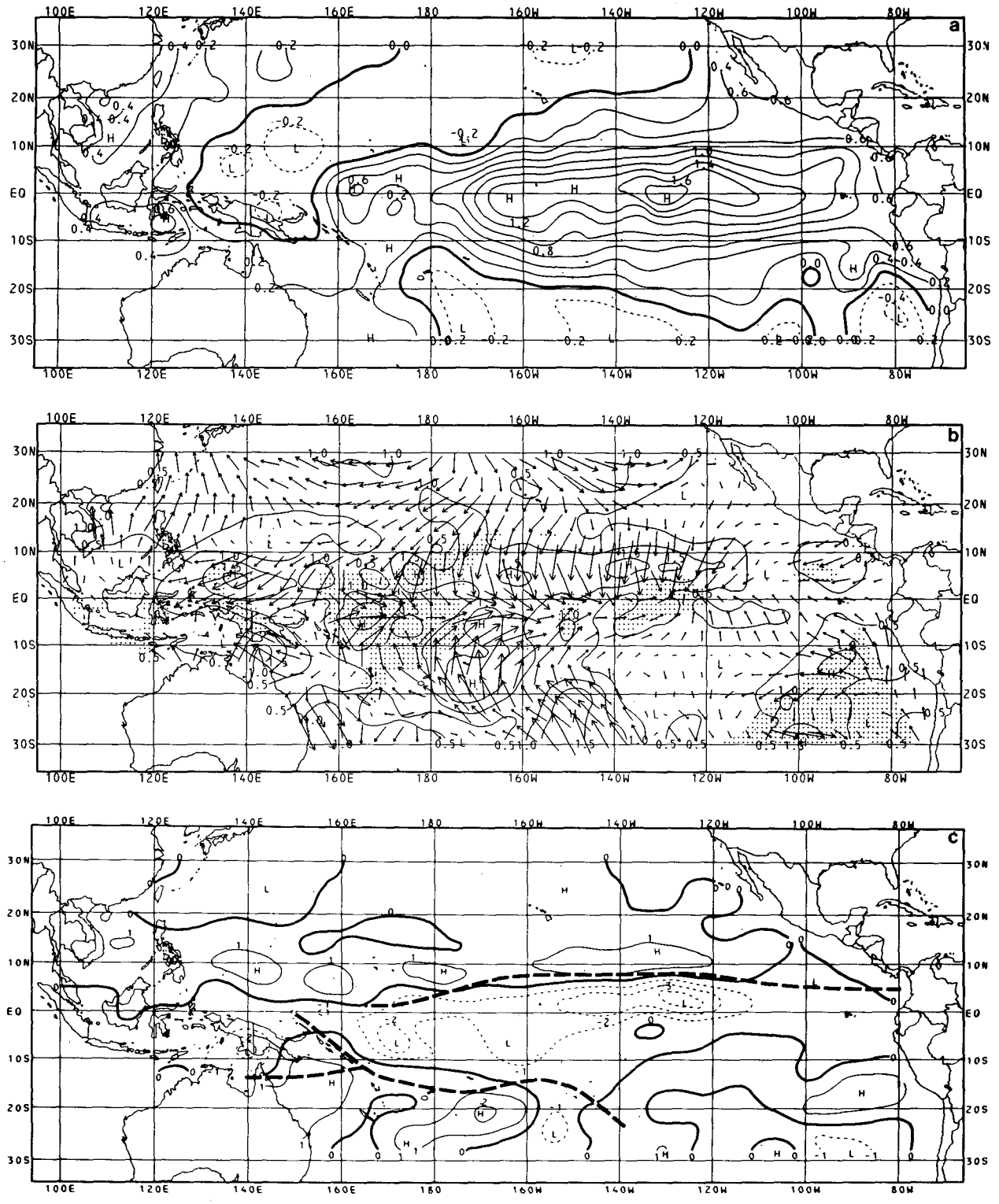

FIG. 21. Mature Phase anomaly composite. (Averages for December–February following El Niño.) Units as in Fig. 17.

general vicinity of the equator. Within this area, our analyses clearly show a phase difference between the variations east and west of 170°W. These two separate areas appear to correspond to the δU_2 and δU_3 maxima of Barnett's Pacific tradewind EOF's (Barnett, 1977b). East of 170°W, the relaxation of the

easterlies lags the warming near the South American coast. West of 170°W, the development of enhanced easterlies, and their demise after October(−1) appears to be consistent with the Wyrtki scenario. The coincidence of these changes with the season of transition from the southwest to northeast monsoon deserves further examination. Recent model computations by Busalacchi and O'Brien (1981) also identify the western rather than the central equatorial Pacific as a prime region of remote forcing.

Because of the potential importance of the wind fluctuations west of the dateline, we have performed a limited case-by-case examination using available data from the area 0–10°N, 140°E–180°, and 0–10°S, 150°E–180°. Data in this area prior to 1953 were too fragmentary for reliable conclusions. Thus we only examined conditions prior to the moderate to strong warm episodes of 1957, 1965, 1969, 1972, 1976 and the weak episode of 1963. The zonal wind anomaly averaged over this area followed the same pattern during all but one (1969) of the six events (Table 3). A predominant pattern of easterly anomalies preceded the warm episodes for periods that varied from a few months (1963) to over three years (1976). A sudden change to westerly anomalies occurred near the end of the year preceding the warm episode. The exceptional event, 1969, was not preceded by easterly anomalies, but the same relative shift, in this case from near zero anomalies to significant westerly anomalies, apparently did occur. This suggests that the anomaly difference between August–September and November–December as well as the anomalies themselves may be an important factor. All extended periods of easterly anomalies between 1954 and 1976 culminated in a warm episode.

The appearance of positive SST anomalies near the dateline around the time of the disappearance of the easterly wind anomalies appears to be a new and perhaps important element in the puzzle. They may arise as a result of diminished upwelling associated with the weakened easterlies.

By September(−1), westerly to northwesterly wind anomalies and positive SST anomalies are spreading into the eastern Pacific south of 15°S, and the surface pressure over that area has fallen below normal seasonal values. As the warming in this area continues, the composites suggest the development of an SST anomaly maximum west of Chile.

TABLE 3. Behavior of average zonal wind anomaly prior to El Niño events in the area 0–10°N, 140°E–180; 0–10°S, 150°E–180.

Year of El Niño	Approximate period of predominant easterly anomalies	Average westerly anomaly (July–September)* ($m\ s^{-1}$)	Average anomaly difference (July–September)* minus (January–March) ($m\ s^{-1}$)
1957	3/54–10/56	−0.7	−0.7
1963	7/62–10/62	−0.3	−1.1
1965	12/63–10/64	−0.9	−1.2
1969	—**	+0.4	−0.8
1972	2/70–11/71	−1.6	−2.4
1976	12/72–1/76	−1.7	−1.8

* Year preceding El Niño.

** Anomalies changed from moderate/weak westerly during early months of 1968 to strong westerly during early months of 1969.

b. Evolution of equatorial wind and SST anomaly fields

The evolution of the SST and wind anomalies along the axis of maximum SST variability is illustrated in Fig. 22. The area of positive SST anomalies which develops near the dateline during November(−1)–December(−1) subsequently spreads both eastward and westward. The rapidly increasing anomalies along the Ecuador–Peru coast spread westward along the equator, merging with the anomaly area near the dateline. This results in small positive SST anomalies during January(0) and February(0) at all longitudes from the South American coast to 150°E. However, positive anomalies continue to intensify near the South American coast, and extend westward along the equator as a relatively narrow tongue of warm water. This more pronounced positive anomaly area continues to expand both westward and latitudinally, with the latitudinal spreading continuing for several months after the occurrence of the peak anomalies on the equator. The reappearance and westward spread of negative anomalies early in the year following El Niño, again as a rather narrow tongue of cold water (Fig. 23), leaves residual positive anomalies at higher latitudes. These gradually disappear with the latitudinal spreading of the negative anomalies. Overall, the lag in the SST anomalies appears to diminish west of 140°W. This is consistent with the small phase differences between ship tracks 5 and 6 described in Section 4c.

Although equatorial SST anomalies are small in the western Pacific, they exhibit a consistent pattern of variation which is opposite in phase to those observed in the eastern equatorial Pacific. Prior to October(−1), when anomalies in the eastern and central Pacific are negative, anomalies west of 150°E are small but positive (0.1–0.3°C). During November(−1)–December(−1), the anomalies in this area change sign as positive anomalies develop near the dateline. Small negative anomalies then persist west of 150°E during the entire period of positive anomalies in the eastern and central Pacific. Around August(+1), at the time when the westward spreading

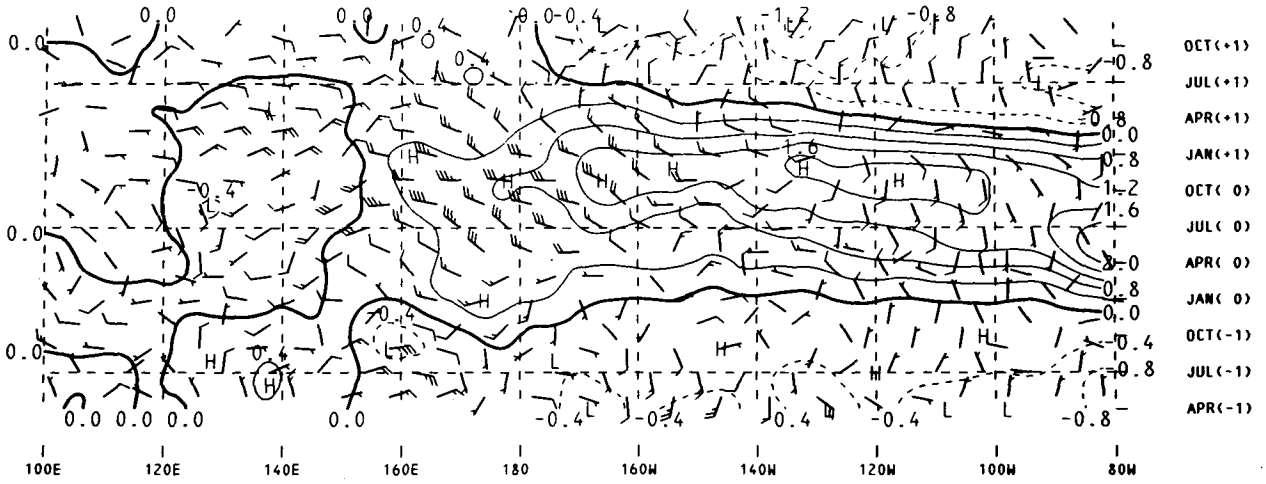

FIG. 22. Time section of composite wind and SST anomalies along the equator (west of 95°W) and axis of maximum SST anomalies (95°W to Peru coast). Units as in Fig. 17.

negative anomalies are approaching the dateline, the anomalies west of 150°E change to small positive values.

Although there is a general tendency for westerlies to the west, and weaker easterlies to the east of the positive SST anomaly along the equator, the phase relationship between the wind and SST anomaly fields appears to change during the warm episode. In the broadest sense, as the area of strongest positive SST anomalies shifts westward, the area of westerly wind anomalies extends eastward. The model results of Gill (1980) are similar in some respects to the anomaly patterns during the Transition and Mature Stages.

The westerly anomalies along the equator reach their maximum eastward extent after the peak SST anomalies, around January(+1). Even then, they extend only to ~130°W. The difference in the phase relationship between SST and U on the three eastern and three western ship tracks, which was discussed in Section 4c and summarized in Table 2, is clearly evident in Fig. 22.

c. Central and eastern Pacific precipitation anomalies

The data indicate large variations in the strength and evolution of the precipitation anomaly pattern from one warm event to another. Thus, the following discussion should be viewed as describing only broadscale mean conditions.

Prior to September(−1), precipitation is below normal over the central equatorial Pacific. A sharp change toward more positive anomalies takes place west of the dateline (Ocean–Nauru Precipitation Index, Fig. 16) during November(−1)–December(−1).

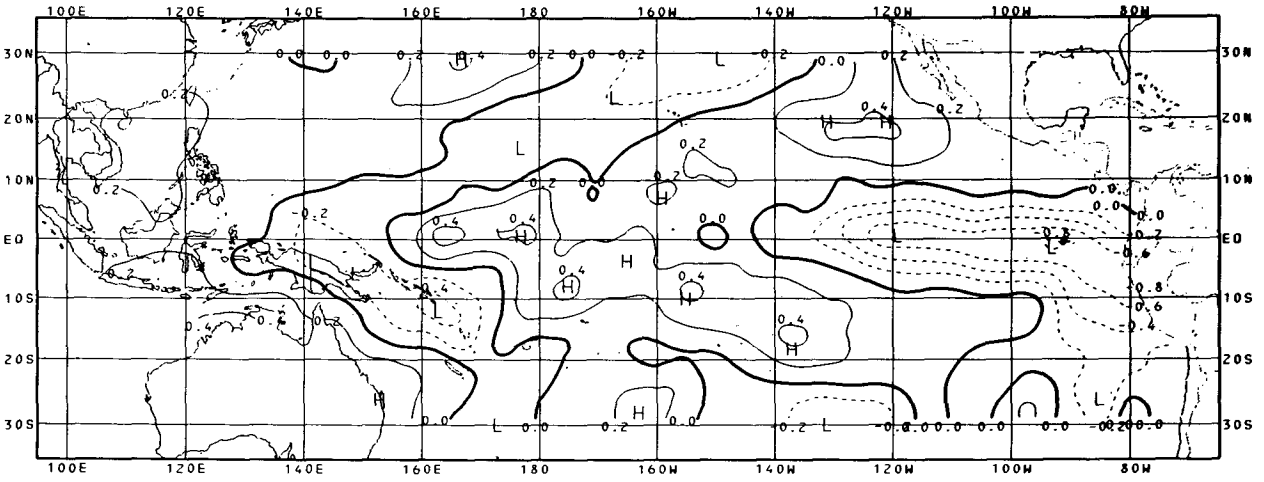

FIG. 23. SST anomaly composite for May–July of year following El Niño.

This appears to be related to the collapse of the easterly wind anomalies west of the dateline, and the development of positive SST anomalies near the dateline. The change to more positive precipitation anomalies reaches the Line Islands around January(0), indicating a typical eastward progression of this feature.

In the eastern equatorial Pacific, positive precipitation anomalies appear in the Galapagos (San Cristobal) around February(0), in association with the appearance of positive SST anomalies, and northerly surface wind anomalies. Since there are no surface stations between the Galapagos and Line Islands, there is some question as to the sequence of events between 90–150°W. However, by April(0) surface convergence anomalies over the central and eastern equatorial Pacific have joined, and the belt of northerly wind anomalies extends westward to 160°W, indicating enhanced precipitation from the South American coast to at least the Nauru–Ocean Island area (165°E).

Precipitation at San Cristobal returns to near normal values in July(0)–August(0), as positive SST anomalies in the area diminish and the seasonal northward movement of the ITCZ places it further from the equator.

By August(0), the precipitation anomalies are concentrated in the central equatorial Pacific, as the southward shift of the ITCZ, coupled with the northeastward shift of the SPCZ erodes the western end of the wedge-shape dry zone from both the north and southwest. Precipitation anomalies peak during August(0)–October(0) at Nauru–Ocean Island and during November(0)–December(0) at the Line Islands. Anomalies at these stations then decrease, becoming negative around June(+1) and reaching minimum values in September(+1)–October(+1).

Krueger and Gray (1969) concluded from satellite data that the dry zone in the eastern Pacific remained relatively intact during the 1965 warm event. However, this apparent inconsistency is easily reconciled with our results, since their conclusion was based on data from December 1965–February 1966. These months correspond to the Mature Phase of the event, when the enhanced precipitation is indeed concentrated in the central equatorial Pacific. Nevertheless, there do appear to be major differences in the precipitation anomaly pattern from event to event. For example, the EOF analysis of Heddinghaus and Krueger (1981), as well as available precipitation reports from San Cristobal, suggest little enhancement of precipitation in the eastern equatorial Pacific during the Peak Phase of the 1976 event.

The question of the relative importance of large-scale vapor flux convergence and enhanced local evaporation as sources of water vapor for the enhanced precipitation in the central Pacific have been examined by a number of authors, e.g., Bjerknes (1969), Cornejo-Garrido and Stone (1977), Ramage *et al.* (1980). The divergence anomaly composites together with typical values of specific humidity (Rasmusson, 1972), can be used to obtain an order of magnitude estimate of the large scale vapor flux divergence contribution. Assuming mean values of 2×10^{-6} s^{-1}, and 14 g kg^{-1} for anomalous convergence and specific humidity through the lowest 150 mb, and neglecting horizontal moisture gradients, yields a value of anomalous vapor flux convergence of 110 mm month^{-1}, similar in magnitude to the precipitation anomalies at Canton and the Line Islands during the Transition and Mature Phases of the warm episode. This supports the conclusion of Cornejo-Garrido and Stone (1977) and Ramage and Hori (1981) that large-scale vapor flux convergence, rather than enhanced local evaporation (Bjerknes, 1969) serves as the main source of water vapor for the enhanced precipitation. The role of enhanced latent and sensible heat fluxes in initiating the circulation anomalies which lead to the vapor flux convergence is another question.

d. Western Pacific precipitation

The western end of the SO/El Niño precipitation seesaw lies in the region of the western Pacific–east Asian monsoon circulations. The Indonesian area is of particular interest since it has been cited as the location of the ascending branch of the Walker Circulation, e.g. Bjerknes (1969), Julian and Chervin (1978). Krishnamurti (1971) and Krishnamurti *et al.* (1973) computed the summer and winter velocity potential fields at 200 mb, which delineate the major regions of ascent and descent of the global time-averaged circulation. These fields clearly reflect both regional meridional and zonal circulation regimes. Viewed in this manner, the Walker Circulation is not an isolated feature, but rather appears as the equatorial portion of a broad-scale east to west divergent flow linking the Asian monsoon regions of mean upward motion to the subsidence regions of the eastern and central Pacific.

Because of its location on the edge of our analysis region, and the local effects associated with the many large islands of the archipelago, we do not consider our divergence composites to be entirely reliable over the Indonesian area. We therefore analyzed precipitation data from 26 stations scattered throughout the area 10°N–10°S, 95–160°E. Some of these records extend as far back as 1879, although there were large gaps in the Indonesian station data after 1960. Warm episodes during the periods 1921–38 and 1949–76 were identified from our SST analysis. Warm episodes during the period 1879–1920 and 1939–48 were equated with the years of moderate or strong El Niño reported by Quinn *et al.* (1978). Warm episode precipitation composites were con-

TABLE 4. El Niño composite precipitation for seven Indonesian stations.*

Month	Average departure (mm)	Percent departure
Jun(−1)	22.8	11.1
Jul(−1)	18.2	10.8
Aug(−1)	24.1	17.4
Sep(−1)	5.4	4.5
Oct(−1)	21.5	15.9
Nov(−1)	17.1	9.2
Dec (−1)	9.7	3.7
Jan(0)	−18.9	−6.3
Feb(0)	−21.0	−8.1
Mar(0)	−20.1	−7.8
Apr(0)	−20.2	−9.5
May(0)	−1.0	−0.4
Jun(0)	−30.8	−15.0
Jul(0)	−53.5	−31.6
Aug(0)	−67.4	−48.8
Sep(0)	−45.0	−37.9
Oct(0)	−28.5	−21.0
Nov(0)	−43.9	−23.6
Dec(0)	−4.8	−1.8
Jan(+1)	17.0	5.6
Feb(+1)	24.2	9.4
Mar(+1)	20.6	8.0
Apr(+1)	5.1	2.4
May(+1)	22.5	10.7
Jun(+1)	−4.8	−2.3

* Stations and number of warm episodes: Ambon (3.7°S, 128.2°E) (17); Dili (8.6°S, 125.6°E) (5); Djakarta (6.2°S, 106.8°E) (17); Kajoemas (7.9°S, 114.2°E) (16); Manado (1.5°N, 124.8°E) (17); Manokwari (0.9°S, 134.3°E) (11); Pontianak (0.0, 109.3°E) (17).

structed for each station, using available data from these and adjacent years.

A strikingly similar anomaly pattern was found over most of Indonesia. Comparison of the seven station average anomalies in Table 4 with the central equatorial Pacific precipitation indices (Fig. 16) clearly illustrates the opposition in sign of the precipitation anomalies in the two regions. Specifically:

1) Precipitation over Indonesia drops below normal around December(−1)–January(0), at the time the anomalies at Nauru–Ocean Island become positive.

2) Maximum negative anomalies occur over Indonesia during July(0)–September(0), at the time of maximum positive anomalies at Nauru–Ocean Island. The coincidence of east monsoon season (May–October) droughts and El Niño years has been pointed out by Quinn *et al.* (1978).

3) Negative anomalies over Indonesia persist for one year, beginning and ending during the west monsoon season. The positive anomalies in the central equatorial Pacific persist a few months longer.

In contrast to most of the Indonesian area, precipitation anomalies over eastern New Guinea show a weak and inconsistent pattern. Nevertheless, this is consistent with the analyses of satellite outgoing longwave radiation data by Heddinghaus and Krueger (1981). Their EOF analysis shows the nodal line between the out-of-phase Indonesian and central Pacific anomaly areas passing just east of New Guinea.

North and east of the main Indonesian archipelago, i.e., northern Borneo, the Phillipines, and the Marshall and Caroline Islands, the most pronounced decrease in precipitation occurs during September(0)–April(1). As discussed in Section 5, this corresponds with the period of weakened northeast monsoon (Fig. 21), a feature which is particularly evident north of 10°N. According to Murakami and Unninayar (1977), the Asian winter monsoon involves a direct meridional circulation over eastern Asia. Associated with this "local Hadley cell" are the southward moving cold surface outbreaks from the Siberian high, rising motion in the region of heavy tropical rainfall, and a vigorous upper tropospheric return current subsiding north of the intense subtropical jetstream near Japan. The weakened northeast monsoon at this stage of the warm episode suggests changes in strength or configuration of the local Hadley cell, which may be related, in turn, to the 200 mb wind anomalies described by Arkin, *et al.* (1980).

e. Midlatitude links

The composites exhibit features which are clearly linked with or extensions of circulation anomalies in higher latitudes. Chen (pers. comm., 1981) has constructed composites comparable to those shown in Section 5 for the surface pressure field north of 20°N. In the overlap region 20–30°N, the major features of the wind and pressure anomaly composites are consistent. Specifically:

1) The area of anomalous cyclonic flow near the dateline which appears on the Onset Phase composite (Fig. 18) reflects the equatorward extension of a low pressure anomaly centered near 25°N, 170°W.

2) An area of cyclonic flow appearing on the Peak Phase composite (Fig. 19) is part of the anomalous circulation around a large midlatitude low-pressure anomaly centered near 35°N, 160°W.

3) Similarly, the pronounced anticyclonic anomalous flow west of the dateline and cyclonic anomalous flow east of the dateline between 20–30°N on the Mature Phase composite (Fig. 20) reflect the circulation around midlatitude high-pressure (35°N–170°E) and low-pressure (45°N, 135°W) anomalies.

In the Southern Hemisphere, the weakening of the high pressure ridge during the warm episode sug-

gests an associated decrease of the middle latitude westerlies on its southern flank. Trenberth (1976) drew the implication of a relationship between the SO and the Southern Hemisphere westerlies from the analysis of Kidson (1975). The recent study of van Loon and Madden (1981) provides evidence that the decrease of the westerlies south of the ridgeline is but one aspect of a large-scale system of SO related anomalies in the higher latitudes of the Southern Hemisphere.

f. Concluding remarks

One must, of course, interpret the composite analyses with some degree of caution. At best, they reflect the common features of six significant warm events which occurred over a period of little more than two decades. The results are undoubtedly biased toward the stronger of the six events, and in some cases may be unduly influenced by a single event. These reservations notwithstanding, the broadscale features of the composites are surprisingly consistent and in good agreement with many other sources of information. The time/space consistency is even more apparent in the full set of three-month running mean composites.

The results of the composite analyses are consistent with a number of results from earlier statistical and case studies. The tendency for enhanced surface convergence in the central Pacific and enhanced divergence in the subtropics shown on the Peak, Transition and Mature Phase composite, is consistent with negative precipitation correlations between Apia and the Line Islands (Doberitz, 1968) and between the Line Islands and Hawaii wintertime precipitation (Meisner, 1976; Wright, 1977). Using the surface wind data of Wyrtki and Meyers (1976), Reiter (1978) found a striking in-phase relationship between the Line Island Precipitation Index and the equatorward flow averaged over broad areas of each hemisphere. His results appear to be consistent with these three wind and divergence anomaly composites. The shift of the SPCZ is consistent with the results of Krueger and Gray (1969), Trenberth (1976) and Heddinghaus and Krueger (1981), and with the finding of Streten (1973) that the SPCZ shifted westward between mid-1969, a warm episode year, and 1971.

Barnett (1981) used advanced statistical techniques to study the relationships between selected ocean and atmospheric variables in the tropical Pacific Ocean. Many of his statistical results can be clearly related to the evolution of SST, wind and pressure fields described in this paper. Examples include the SST lag relationship between South American coastal stations and Christmas Island, the increase (decrease) in the equatorward component of the winds in both hemispheres when western equatorial SST anomalies are positive (negative), the importance of the wind variations in the central and western equatorial Pacific and the lag relationship between the Darwin minus Easter Island SOI and SST's at South American coastal stations. Pazan and Meyers (1982) have recently analyzed SO-related wind variations by linearly correlating the wind variations at each grid point with Wright's SOI (Wright, 1977). Many of the features revealed by our composites also appear in their analysis.

Some aspects of the surface wind anomaly fields can be described in terms of the simple equatorial Walker Circulation model first proposed by Bjerknes (1969). However, the model constitutes an incomplete description of the SST, wind and precipitation anomaly fields during the warm episodes. It relates anomalous precipitation to variations of the zonal wind component near the equator and the local meridional circulation anomaly, rather than describing them in terms of the southward shift of the ITCZ and the northeastward shift of the SPCZ, which are the critical kinematic features associated with the central Pacific precipitation anomaly pattern. It does not adequately address the circulation variations in the Southwest Pacific, the link with the northeast monsoon, or the striking evolution of the anomaly fields.

The results of this study clearly show that the SO and the associated warm episodes cannot be adequately described in terms of standing oscillations. The significant phase differences from one area to another and the locally varying wind/SST phase relationships are essential elements in the description and understanding of this phenomenon. Documentation of these phase differences is of utmost importance for the development of empirical prediction relationships. Of the six episodes studied, only one of the weaker events (1951) did not exhibit a strong follow-through in the central Pacific during the northern winter following El Niño, and this result is open to question in view of the poor central Pacific data at that time. Similarly, only one significant wintertime warm episode in the central Pacific (1963) did not exhibit large positive anomalies on the Peru coast several months earlier. Thus, large positive SST anomalies along the Peru Coast during April–June were usually followed by significant positive SST and precipitation anomalies in the central Pacific during the following northern winter. Conversely, large positive SST anomalies are unlikely in the central Pacific during the northern winter, when teleconnections with the Northern Hemisphere extratropics are strongest (Horel and Wallace, 1981; Trenberth and Paolino, 1981; Arkin, *et al.*, 1980), unless they are preceded by large positive anomalies on the Peru Coast several months earlier.

Acknowledgments. This investigation was greatly stimulated by many discussions with Dr. Joseph Fletcher, Deputy Director, Environmental Research Laboratories, in which he generously made available his unpublished results. It is a pleasure to acknowledge our debt and appreciation to him. We wish to express our appreciation to Dr. Thomas H. Austin, retired Director, Environmental Data and Information Services, and Dr. Joshua Z. Holland, former Director, Center for Environmental Assessment Services, for their enthusiastic support during the early stages of this study, and to Dr. Jay S. Winston, Director, Climate Analysis Center, for his encouragement, support and suggestions during the later stages of the work.

Special thanks are due Mr. Rob Quayle, National Climatic Center, for his efforts in developing the surface marine data set on which much of this study is based. Prof. William Quinn, Oregon State University, provided key station pressure and coastal station SST data. Mr. John Horel, University of Washington, supplied important precipitation composite data.

We are deeply indebted to Prof. John M. Wallace, University of Washington, for many stimulating discussions and a host of constructive suggestions. We have also benefitted from discussions with many other colleagues, particularly Mr. Arthur F. Krueger, Mr. Phillip Arkin and Dr. Wilbur Chen, Climate Analysis Center, and Dr. George Philander, Geophysical Fluid Dynamics Laboratory.

We express our appreciation to Mr. John Kopman, who prepared a number of illustrations, and Ms. Gail Lucas for typing the manuscript. This work was partially supported by the Equatorial Pacific Ocean Climate Studies (EPOCS). This is EPOCS Contribution No. 12.

APPENDIX

Sources of Data for Compacted Pacific Marine Data Set (National Climatic Center)

Source deck	Original source	General period of record
110	U.S. Navy Marine Observations	1945–51
116	U.S. Merchant Marine	1949–63
118	Japanese Ship Observations No. 1	1933–53
119	Japanese Ship Observations No. 2	1953–61
128	International Marine Observations	1963
281	U.S. Navy MAR Marine Observations	1920–45
184	Great Britain Marine Observations	1953–56
185	U.S.S.R. Marine Synoptic Observations	1957–58
187	Japanese Whaling Fleet Observations	1946–56
188	Norwegian Whaling Fleet Observations	1932–39
189	Netherlands Marine Observations	1939–55
192	Deutsche Seewarte Marine Observations	1859–1939
193	Netherlands Marine Observations	1854–1938
194	Great Britain Marine Observations	1856–1953
195	U.S. Navy Ship Logs	1942–45
196	Deutsche Seewarte Marine Observations	1949–54
197	Danish Marine Observations (Arctic and Antarctic)	1860–1956
902	Great Britain 184 extension	1959–62
186	U.S.S.R. Ice Island Observations	1937, 1950–70
666	Tuna Reports (Fisheries)	1960–75
891	Surface data taken in conjunction with oceanographic soundings (NODC)	1880–
888	AFGWC Telecommunications	1973–
890	NMC Telecommunications	1976–
150	Netherlands HSST	1861–1960
151	German HSST	1861–1960
152	U.K. HSST	1861–1960

REFERENCES

Arkin, P. A., W. Y. Chen and E. M. Rasmusson, 1980: Fluctuations in mid and upper tropospheric flow associated with the Southern Oscillation. *Proc. Fifth Ann. Clim. Diag. Workshop*, U.S. Dept. of Commerce, Washington, DC. [NTIS PB-81-222200].

Barnett, T. P., 1977a: An attempt to verify some theories of El Niño. *J. Phys. Oceanogr.*, **7**, 633–647.

——, 1977b: The principal time and space scales of the Pacific Tradewind field. *J. Atmos. Sci.*, **34**, 221–236.

——, 1981: Statistical relations between ocean/atmosphere fluctuations in the tropical Pacific. *J. Phys. Oceanogr.*, **11**, 1043–1058.

Berlage, H. P., 1957: Fluctuations in the general atmospheric circulation of more than one year, their nature and prognostic value. *K. Ned. Meteor. Inst., Meded. Verh.*, **69**, 152 pp.

——, 1966: The Southern Oscillation and world weather. *K. Ned. Meteorol. Inst., Meded. Verh.*, **88**, 152 pp.

Bjerknes, J., 1966: A possible response of the atmospheric Hadley circulation to equatorial anomalies of ocean temperature. *Tellus*, **18**, 820–829.

——, 1969: Atmospheric teleconnections from the equatorial Pacific. *Mon. Wea. Rev.*, **97**, 163–172.

——, 1972: Large-scale atmospheric response to the 1964–65 Pacific equatorial warming. *J. Phys. Oceanogr.*, **2**, 212–217.

Busalacchi, A., and J. J. O'Brien, 1981: Interannual variability of the equatorial Pacific in the 1960's. *J. Geophys. Res.*, **86**, 10901–10907.

Chen, W. Y., 1982: Assessment of Southern Oscillation sea level pressure indices. *Mon. Wea. Rev.*, **110** (in press).

Collins, C. A., L. F. Giovando and K. B. Abbott-Smith, 1975: Comparison of Canadian and Japanese merchant-ship ob-

servations of sea-surface temperature in the vicinity of present Ocean Weather Ship "P", 1927-33. *J. Fish. Res. Board Can.*, **32,** 253-258.

Cornejo-Garrido, A. G., and P. H. Stone, 1977: On the heat balance of the Walker Circulation. *J. Atmos. Sci.*, **34,** 1155-1162.

Doberitz, R., 1968: Cross spectrum analysis of rainfall and sea temperature of the equatorial Pacific Ocean. *Bonner Meteor. Abhand.*, **8,** 61 pp.

Donguy, J. R., and C. Henin, 1980a: Surface conditions in the eastern equatorial Pacific related to the intertropical convergence zone of the winds. *Deep-Sea Res.*, **27A,** 693-714.

——, and ——, 1980b: Climatic teleconnections in the western South Pacific with El Niño phenomenon. *J. Phys. Oceanogr.*, **10,** 1952-1958.

Enfield, D. B., 1980: El Niño-Pacific eastern boundary response to interannual forcing. *Resource Management and Environmental Uncertainty*, M. H. Glantz, Ed., Wiley, 213-254.

——, 1981a: Thermally driven wind variability in the planetary boundary layer above Lima, Peru. *J. Geophys. Res.*, **86,** 2005-2016.

——, 1981b: Annual and nonseasonal variability of monthly low-level wind fields over the southeastern tropical Pacific. *Mon. Wea. Rev.*, **109,** 2177-2190.

Gill, A. E., 1980: Some simple solutions for heat-induced tropical circulation. *Quart. J. Roy. Meteor. Soc.*, **106,** 447-462.

Goldenberg, S. B., and J. J. O'Brien, 1981: Time and space variability of tropical Pacific wind stress. *Mon. Wea. Rev.*, **109,** 1190-1207.

Heddinghaus, T. R., and A. F. Krueger, 1981: Annual and interannual variations in outgoing longwave radiation over the tropics. *Mon. Wea. Rev.*, **109,** 1208-1218.

Hickey, B., 1975: The relationship between fluctuations in sea level, wind stress and sea surface temperature in the equatorial Pacific. *J. Phys. Oceanogr.*, **5,** 460-475.

Hildebrandsson, H. H., 1897: Quelques recherches sur les entres d'action de l'atmosphere. *K. Svenska Vetens.-Akad. Handl.*, **29,** 33 pp.

Horel, J. D., and J. M. Wallace, 1981: Planetary scale atmospheric phenomena associated with the Southern Oscillation. *Mon. Wea. Rev.*, **109,** 813-829.

Hoskins, B. J., and D. J. Karoly, 1981: The steady linear response of a spherical atmosphere in thermal and orographic forcing. *J. Atmos. Sci.*, **38,** 1179-1196.

Hurlburt, H. E., J. C. Kindle and J. J. O'Brien, 1976: A numerical simulation of the onset of El Niño. *J. Phys. Oceanogr.*, **6,** 621-631.

Jenkins, G. M., and D. G. Watts, 1968: *Spectral Analysis and Its Applications.* Holden-Day, 379-381.

Julian, P. R., 1971: Some aspects of variance spectra of synoptic scale tropospheric wind components in midlatitudes and in the tropics. *Mon. Wea. Rev.*, **99,** 954-965.

——, 1975: Comments on the determination of significance levels of the coherence statistics. *J. Atmos. Sci.*, **32,** 836-837.

——, and R. M. Chervin, 1978: A study of the Southern Oscillation and Walker Circulation phenomenon. *J. Atmos. Sci.*, **106,** 1433-1451.

Keshavamurty, R. N., 1982: Response of the atmosphere to sea surface temperature anomalies over the equatorial Pacific and the teleconnections of the Southern Oscillation. *J. Atmos. Sci.*, **39** (in press).

Kidson, J. W., 1975: Tropical eigenvector analysis and the Southern Oscillation. *Mon. Wea. Rev.*, **103,** 187-196.

Krishnamurti, T. N., 1971: Tropical east-west circulations during the northern summer. *J. Atmos. Sci.*, **28,** 1342-1347.

——, M. Kanamitsu, W. J. Koss and J. D. Lee, 1973: Tropical east-west circulations during the northern winter. *J. Atmos. Sci.*, **30,** 780-787.

Krueger, A. F., and J. S. Winston, 1974: A comparison of the flow over the tropics during two contrasting circulation regimes. *J. Atmos. Sci.*, **31,** 358-370.

——, and ——, 1975: Large scale circulation anomalies over the tropics during 1971-1972. *Mon. Wea. Rev.*, **103,** 465-473.

——, and ——, 1979: Further analysis of recent fluctuations in circulation and cloudiness (rainfall) over the tropics. *Proc. Fourth Ann. Clim. Diag. Workshop*, U.S. Department of Commerce, Washington, DC, 84-93. [NTIS PB-201130].

——, and T. Gray, 1969: Long-term variations in equatorial circulation and rainfall. *Mon. Wea. Rev.*, **97,** 700-711.

Lau, K-M., 1981: Oscillations in a simple equatorial climate system. *J. Atmos. Sci.*, **38,** 248-261.

Lockyer, N., and W. J. S. Lockyer, 1902a: On some phenomena which suggest a short period of solar and meteorological changes. *Proc. Roy. Soc. London*, **70,** 500.

——, and ——, 1902b: On the similarity of the short-period pressure variation over large areas. *Proc. Roy. Soc. London*, **71,** 134-135.

——, and ——, 1904: The behaviour of the short-period atmospheric pressure variation over the earth's surface. *Proc. Roy. Soc. London*, **73,** 457-470.

Lockyer, W. J. S., 1906: Barometric variations of long duration over large areas. *Proc. Roy. Soc. London*, **A78,** 43-60.

McCreary, J., 1976: Eastern tropical ocean response to changing wind systems: With application to El Niño. *J. Phys. Oceanogr.*, **6,** 632-645.

McWilliams, J. C., and P. R. Gent, 1978: A coupled air-sea model for the tropical Pacific. *J. Atmos. Sci.*, **35,** 962-989.

Meisner, B. N., 1976: A study of Hawaiian and Line Island rainfall. Rep. UHMET 76-4, Dep. Meteor., University of Hawaii, Honolulu, 83 pp.

Murakami, T., and M. S. Unninayar, 1977: Atmospheric circulation during December 1970 through February 1971. *Mon. Wea. Rev.*, **105,** 1024-1038.

Namias, J., 1976: Some statistical and synoptic characteristics associated with El Niño, *J. Phys. Oceanogr.*, **6,** 130-138.

O'Brien, J. J., A. Busalacchi and J. Kindle, 1980: Ocean models of El Niño. *Resource Management and Environmental Uncertainty*, M. H. Glantz, Ed., Wiley, 159-212.

Opsteegh, J. D., and H. M. Van den Dool, 1980: Seasonal differences in the stationary response of a linearized primitive equation model: Prospects for long range forecasting? *J. Atmos. Sci.*, **37,** 2169-2185.

Pazan, S., and G. Meyers, 1982: Interannual fluctuations of the tropical Pacific wind field and the Southern Oscillation. *Mon. Wea. Rev.*, **110,** 587-600.

Philander, S. G. H., 1981: The response of equatorial oceans to a relaxation of the trade winds. *J. Phys. Oceanogr.*, **11,** 176-189.

Pittock, A. B., 1975: Climatic change and the patterns of variation in Australian rainfall. *Search*, **6,** 498-504.

Quinn, W. H., 1979: Monitoring and predicting short-term climate changes in the South Pacific Ocean. *Proc. Int. Conf. on Mar. Sci. and Tech., Part 1*, Catholic University of Valparaiso, Valparaiso, Chile, 26-30.

——, D. O. Zopf, K. S. Short and R. T. W. Kuo Yang, 1978: Historical trends and statistics of the Southern Oscillation, El Niño, and Indonesian droughts. *Fish. Bull.*, **76,** 663-678.

Rabiner, L. R., M. R. Sambur and C. E. Schmidt, 1975: Applications of a nonlinear smoothing algorithm to speech processing. *IEEE Trans. on Acoust. Speech Signal Process.*, **ASSP-23,** 552-557.

Ramage, C. S., 1975: Preliminary discussion of the meteorology of the 1972-73 El Niño. *Bull. Amer. Meteor. Soc.*, **56,** 234-242.

——, C. W. Adams, A. M. Hori, B. J. Kilonsky and J. C. Sadler, 1980: Meteorological atlas of the 1972-73 El Niño. UHMET 80-03, Dep. Meteorology, University of Hawaii, Honolulu, 101 pp.

——, and A. M. Hori, 1981: Meteorological aspects of El Niño. *Mon. Wea. Rev.*, **109,** 1827-1835.

Rasmusson, E. M., 1972: Seasonal variation in tropical humidity parameters. *The General Circulation of the Tropical At-*

mosphere and Interactions with Extratropical Latitudes, Vol. 1, R. E. Newell, J. W. Kidson, D. G. Vincent and G. Boer, Eds., MIT Press, pp. 193–237.

——, and T. H. Carpenter, 1980: SST lag relationships in the eastern Pacific. *Tropical Ocean–Atmosphere Newsletter*, No. 4, D. Halpern, Ed., NOAA Pacific Marine Environmental Laboratories, Seattle, WA 98105.

——, P. A. Arkin, W. Y. Chen and J. B. Jalickee, 1981: Biennial variations in surface temperature over the United States as revealed by singular decomposition. *Mon. Wea. Rev.*, **109,** 181–192.

Reiter, E. R., 1978: Long-term wind variability in the tropical Pacific, its possible causes and effects. *Mon. Wea. Rev.*, **106,** 324–330.

Rowntree, P. R., 1972: The influence of tropical east Pacific Ocean temperature on the atmosphere. *Quart. J. Roy. Meteor. Soc.*, **98,** 290–321.

Sadler, J. C., 1969: Average cloudiness in the tropics from satellite observations. *International Indian Ocean Expedition Meteor. Monogr.*, No. 2, East-West Center Press, 22 pp.

——, and B. J. Kilonsky, 1981: Tradewind monitoring using satellite observations. Rep. UHMET 81-01, Dep. Meteor., University of Hawaii, Honolulu, 23 pp.

Saur, J. F. T., 1963: A study of the quality of sea water temperatures reported in logs of ships' weather observations. *J. Appl. Meteor.*, **2,** 417–425.

Streten, N. A., 1973: Some characteristics of satellite-observed bands of persistent cloudiness over the Southern Hemisphere. *Mon. Wea. Rev.*, **101,** 486–495.

Tabata, S., 1978: An evaluation of the quality of sea surface temperatures and salinities measured at station P and line P in the northeast Pacific Ocean. *J. Phys. Oceanogr.*, **8,** 970–986.

Taylor, R. C., 1973: An atlas of Pacific island rainfall. Hawaii Inst. Geophys. Data Rep. No. 25, HIG-73-9, 175 pp. [NTIS No. AD 767073].

Trenberth, K. E., 1976: Spatial and temporal variations in the Southern Oscillation. *Quart. J. Roy. Meteor. Soc.*, **102,** 639–653.

——, and D. A. Paolino, Jr., 1981: Characteristic patterns of variability of sea-level pressure in the Northern Hemisphere. *Mon. Wea. Rev.*, **109,** 1169–1189.

Troup, A. J., 1965: The Southern Oscillation. *Quart. J. Roy. Meteor. Soc.*, **91,** 490–506.

van Loon, H., and R. A. Madden, 1981: The Southern Oscillation: Part I: Global associations with pressure and temperature in northern winter. *Mon. Wea. Rev.*, **109,** 1150–1162.

Walker, G. T., 1923: Correlation in seasonal variations of weather, VIII: A preliminary study of world weather. *Mem. Indian Meteor. Dep.*, **24,** 75–131.

——, 1924: Correlation in seasonal variations of weather, IX: A further study of world weather. *Mem. Indian Meteor. Dep.*, **24,** 275–332.

——, 1928: World Weather III. *Mem. Roy. Meteor. Soc.*, **2,** 97–106.

——, and E. W. Bliss, 1930: World Weather IV. *Mem. Roy. Meteor. Soc.*, **3,** 81–95.

——, and ——, 1932: World Weather V. *Mem. Roy. Meteor. Soc.*, **4,** 53–84.

——, and ——, 1937: World Weather VI. *Mem. Roy. Meteor. Soc.*, **4,** 119–139.

Weare, B. C., 1982: El Niño and tropical Pacific Ocean temperatures. *J. Phys. Oceanogr.*, **12,** 17–27.

——, A. R. Navato and R. E. Newell, 1976: Empirical orthogonal analysis of Pacific sea surface temperatures. *J. Phys. Oceanogr.*, **6,** 671–678.

Webster, P. S., 1981: Mechanisms determining the atmospheric response to sea surface temperature anomalies. *J. Atmos. Sci.*, **38,** 554–571.

Winston, J. S., and A. F. Krueger, 1978: Tropical circulation and radiation fluctuations: interactions with midlatitude circulations during 1976–1978. *Proc. Third Ann. Clim. Diag. Workshop*, U.S. Dep. Commerce, Washington, DC, 16 pp. [NTIS PB298355].

Wooster, W. S., and O. Guillen, 1974: Characteristics of El Niño in 1972. *J. Mar. Res.*, **32,** 378–404.

Wright, P. B., 1977: The Southern Oscillation—patterns and mechanisms of the teleconnections and the persistence. Hawaii Inst. Geophys. Rep. HIG-77-13, 107 pp.

Wyrtki, K., 1964: The thermal structure of the eastern Pacific Ocean. *Dtsch. Hydrogr. Z.*, **A6,** 84 pp.

——, 1965: The annual and semiannual variation of sea surface temperature in the North Pacific Ocean. *Limnol. Oceanogr.*, **10,** 307–313.

——, 1975: El Niño—the dynamic response of the equatorial Pacific Ocean to atmospheric forcing. *J. Phys. Oceanogr.*, **5,** 572–584.

——, 1979a: El Niño. *La Recherche*, **10,** 1212–1220.

——, 1979b: The response of sea level topography to the 1976 El Niño. *J. Phys. Oceanogr.*, **9,** 1223–1231.

——, 1980: Comparison of four equatorial wind indices in the Pacific and El Niño outlook for 1981. *Proc. Fifth Ann. Clim. Diag. Workshop*, U.S. Dep. Commerce, Washington, DC, 211–218. [NTIS PB-81-222200].

——, and G. Meyers, 1976: The trade wind field over the Pacific Ocean. *J. Appl. Meteor.*, **15,** 698–704.